(1 + ∞)-dimensional attractor neural networks

(1 + ∞)-dimensional attractor neural networks

N S Skantzos and A C C Coolen

Department of Mathematics, King's College London, The Strand, London WC2R 2LS, UK

E-mail: skantzos@mth.kcl.ac.uk and tcoolen@mth.kcl.ac.uk

Abstract. We solve a class of attractor neural network models with a mixture of 1D nearest-neighbour interactions and infinite-range interactions, which are both of a Hebbian-type form. Our solution is based on a combination of mean-field methods, transfer matrices, and 1D random-field techniques, and is obtained both for Boltzmann-type equilibrium (following sequential Glauber dynamics) and Peretto-type equilibrium (following parallel dynamics). Competition between the alignment forces mediated via short-range interactions, and those mediated via infinite-range ones, is found to generate novel phenomena, such as multiple locally stable 'pure' states, first-order transitions between recall states, 2-cycles and non-recall states, and domain formation leading to extremely long relaxation times. We test our results against numerical simulations and simple benchmark cases, and find excellent agreement.

1. Introduction

Solvable models of recurrent neural networks are bound to be simplified representations of biological reality. The early statistical mechanical studies of such networks, e.g. [1, 2], concerned mean-field models, whose statics and dynamics are by now well understood, and have obtained the status of textbook material [3]. The focus in theoretical research has consequently turned to new areas, such as solving the dynamics of large recurrent networks close to saturation [4], the analysis of finite size phenomenology [5], solving biologically more realistic models [6], or networks with spatial structure [7–11]. In this paper we analyse Ising spin models of recurrent networks with spatial structure, in which there are two coexistent classes of Hopfield-type [1] interactions: infinite-range ones (operating between any pair of neurons), and 1D short-range ones (operating between nearest neighbours only). The study of this type of structure is motivated by the interplay typically observed in cortical tissue between long-range processing via pyramidal neurons and short-range processing via either excitatory pyramidal cells or inhibitory interneurons. Indeed, as current evidence suggests in most cortical areas the interactions are positive at the very short range, on a slightly larger range inhibitory and again predominantly positive on the very large range.

Due to the presence of short-range interactions however, and in contrast to early papers on spatially structured networks, solutions based solely on simple mean-field approaches are ruled out. The analysis requires significantly more complicated methods and the present models can be solved exactly only by a combination of mean- and random-field techniques [12–16], whereas for the special case in which the system has stored a single pattern, a simple (Mattis) transformation allows us to derive the solution via a combination of mean-field methods and transfer matrices.

This paper is organised as follows. We first solve the one-pattern case in which pattern variables can be transformed away (thus providing a convenient and exactly solvable benchmark case against which to test the general theory). This also hints at the interesting features induced by short- versus long-range competition in the more general model. In particular, already in the one-pattern model we find first-order phase transitions, regimes corresponding to multiple locally stable states and we find that sequential and parallel dynamics phase diagrams are related by simple transformations. We then proceed to the general case, with an arbitrary number of stored patterns, away from saturation regimes. For sequential dynamics (Boltzmann equilibrium) we adapt the 1D random-field techniques as originally developed for site-disordered Ising chains, and combine them with mean-field methods; for parallel dynamics (Peretto equilibrium) we adapt and combine with mean-field methods the procedure in [16], based on 4×4 random transfer matrices. The disorder-averaged free energy and the order parameters are found, in closed and exact form, as integrals over the distribution of a characteristic variable, which represents a specific ratio of conditioned partition functions. This distribution is calculated following [12, 13].

In the region where the infinite- versus short-range competition is prominent, our theory predicts a *series* of (continuous and discontinuous) dynamic phase transitions, and a free-energy surface with multiple local minima. These features become more prominent, in both number and strength, when the number of stored patterns increases, in sharp contrast to Hopfield-type infinite-range networks [1], where 'pure state' solutions are independent of the number of patterns stored. The transition lines of sequential and parallel dynamics phase diagrams are found to be related by reflection symmetries and also parallel dynamics macroscopic equations can describe 2-cycles rather than fixed-points solutions. Finally we test our theory against several exactly solvable cases and against numerical simulations; the latter are found to exhibit interesting but extremely slow domain-induced dynamics, with plateau phases. Once equilibration has occurred, we obtain excellent agreement between theory and experiment.

2. Model definitions

We study models with N Ising spin neuron variables $\boldsymbol{\sigma} = (\sigma_1, \ldots, \sigma_N) \in \{-1, 1\}^N$, which evolve in time stochastically on the basis of post-synaptic potentials $h_i(\boldsymbol{\sigma})$ (or local fields), following the Glauber-type rule

$$\text{Prob}[\sigma_i(t+1) = \pm 1] = \tfrac{1}{2}[1 \pm \tanh[\beta h_i(\boldsymbol{\sigma}(t))]] \qquad h_i(\boldsymbol{\sigma}) = \sum_{j \neq i} J_{ij}\sigma_j + \theta_i. \tag{1}$$

The parameters J_{ij} and θ_i represent synaptic interactions and firing thresholds. The (non-negative) parameter β controls the amount of noise, with $\beta = 0$ and ∞ corresponding to purely random and purely deterministic response, respectively. If the interaction matrix is symmetric, both a random sequential execution and a fully parallel execution of the stochastic dynamics (1) will evolve to a unique equilibrium state. The corresponding microscopic state probabilities can both formally be written in the Boltzmann form $p_\infty(\boldsymbol{\sigma}) \sim \exp[-\beta H(\boldsymbol{\sigma})]$, with associated Hamiltonians [1, 17] (since Peretto's pseudo-Hamiltonian H_{par} depends on β, the associated statistics are not of the Boltzmann form):

$$H_{\text{seq}}(\boldsymbol{\sigma}) = -\tfrac{1}{2} \sum_{i \neq j} \sigma_i J_{ij} \sigma_j - \sum_i \theta_i \sigma_i \tag{2}$$

$$H_{\text{par}}(\boldsymbol{\sigma}) = -\frac{1}{\beta} \sum_i \log 2 \cosh[\beta h_i(\boldsymbol{\sigma})] - \sum_i \theta_i \sigma_i. \tag{3}$$

In both cases, expectation values of order parameters can be obtained by differentiation of the free energy per neuron $f = -\lim_{N \to \infty} (\beta N)^{-1} \log \sum_{\boldsymbol{\sigma}} \exp[-\beta H(\boldsymbol{\sigma})]$, which acts as a

generating function. For the parameters J_{ij} and θ_i we now make the following choice†:

$$
J_{ij} = \frac{J_{ij}^\ell}{N} + J_{ij}^s (\delta_{i,j+1} + \delta_{i,j-1}) \qquad \theta_i = \theta
$$

$$
J_{ij}^\ell = J_\ell^{(1)} + J_\ell^{(2)} \sum_{\mu=1}^p \xi_i^\mu \xi_j^\mu \qquad J_{ij}^s = J_s^{(1)} + J_s^{(2)} \sum_{\mu=1}^p \xi_i^\mu \xi_j^\mu. \tag{4}
$$

This corresponds to the result of having stored a set of binary patterns $\{\boldsymbol{\xi}^1, \ldots, \boldsymbol{\xi}^p\}$ with $\xi_i^\mu \in \{-1, 1\}$ in a 1D chain of neurons, through Hebbian-type learning, but with different (potentially conflicting) embedding strengths $J_s^{(2)}$ and $J_\ell^{(2)}$ associated with the short-range versus the infinite-range interactions. We will choose $p \ll N$. The parameters $J_s^{(1)}$ and $J_\ell^{(1)}$ control uniform contributions to the interactions within their class. Taking derivatives of f with respect to $J_\ell^{(2)}$ produces expressions involving the familiar 'overlap' order parameters:

$$
\text{sequential:} \quad \boldsymbol{m}^2 = -2 \frac{\partial f}{\partial J_\ell^{(2)}} = \lim_{N \to \infty} \left\langle \left(\frac{1}{N} \sum_i \sigma_i \boldsymbol{\xi}_i \right)^2 \right\rangle_{\text{eq}}
$$

$$
\text{parallel:} \qquad \boldsymbol{m}^2 = -\frac{\partial f}{\partial J_\ell^{(2)}} = \lim_{N \to \infty} \left\langle \left(\frac{1}{N} \sum_i \sigma_i \boldsymbol{\xi}_i \right)^2 \right\rangle_{\text{eq}}
$$

where the brackets $\langle \cdots \rangle_{\text{eq}}$ denote equilibrium averages, $\boldsymbol{m} = (m_1, \ldots, m_p)$, and $\boldsymbol{x}_i \cdot \boldsymbol{x}_j = \sum_\mu x_i^\mu x_j^\mu$. Note that for $J_s^{(2)} = J_\ell^{(2)} = 0$ we obtain the simpler model

$$
J_{ij} = \frac{J_\ell}{N} + J_s (\delta_{i,j+1} + \delta_{i,j-1}) \qquad \theta_i = \theta. \tag{5}
$$

The Mattis transformation $\sigma_i \to \sigma_i \xi_i$ maps this model onto

$$
J_{ij} = \frac{J_\ell}{N} \xi_i \xi_j + J_s (\delta_{i,j+1} + \delta_{i,j-1}) \xi_i \xi_j \qquad \theta_i = \theta \xi_i \tag{6}
$$

which corresponds to the result of having stored just a single pattern $\boldsymbol{\xi} = (\xi_1, \ldots, \xi_N) \in \{-1, 1\}^N$. Taking derivatives of f with respect to the parameters θ and J_s in (5) produces our order parameters:

$$
\text{sequential:} \quad m = -\frac{\partial f}{\partial \theta} = \lim_{N \to \infty} \frac{1}{N} \sum_i \langle \sigma_i \rangle_{\text{eq}}
$$

$$
a = -\frac{\partial f}{\partial J_s} = \lim_{N \to \infty} \frac{1}{N} \sum_i \langle \sigma_{i+1} \sigma_i \rangle_{\text{eq}}
$$

$$
\text{parallel:} \qquad m = -\frac{1}{2} \frac{\partial f}{\partial \theta} = \lim_{N \to \infty} \frac{1}{N} \sum_i \langle \sigma_i \rangle_{\text{eq}}
$$

$$
a = -\frac{1}{2} \frac{\partial f}{\partial J_s} = \lim_{N \to \infty} \frac{1}{N} \sum_i \langle \sigma_{i+1} \tanh[\beta h_i(\boldsymbol{\sigma})] \rangle_{\text{eq}}
$$

where we have simplified the parallel dynamics observables with the identities

$$
\langle \sigma_{i+1} \tanh[\beta h_i(\boldsymbol{\sigma})] \rangle_{\text{eq}} = \langle \sigma_{i-1} \tanh[\beta h_i(\boldsymbol{\sigma})] \rangle_{\text{eq}} \qquad \text{and} \qquad \langle \tanh[\beta h_i(\boldsymbol{\sigma})] \rangle_{\text{eq}} = \langle \sigma_i \rangle_{\text{eq}}
$$

which follow from (1) and from invariance under the transformation $i \to N + 1 - i$ (for all i). For model (5) m is the average neuronal activity. For sequential dynamics a describes the average equilibrium state covariances of neighbouring neurons, and for parallel dynamics it gives the average equilibrium state covariances of neurons *at a given time t*, and their

† Competition between a different type of uniform infinite-range and random nearest-neighbour interactions has been studied recently in [19], for sequential dynamics only.

neighbours *at time t* + 1 (the difference between the two meanings of *a* will be important in the presence of 2-cycles). For model (6) one similarly finds

$$m = \lim_{N\to\infty} \frac{1}{N} \sum_i \langle \xi_i \sigma_i \rangle_{\text{eq}} \qquad a = \lim_{N\to\infty} \frac{1}{N} \sum_i \langle (\xi_i \sigma_i)(\xi_{i+1}\sigma_{i+1}) \rangle_{\text{eq}}.$$

The observable *m* is here the familiar overlap order parameter of associative memory models [1, 2], which measures the quality of pattern recall in equilibrium. Note that $m, a \in [-1, 1]$.

3. Solution and phase diagrams for $p = 1$

Before we proceed to the solution of the general model (4) we first solve the relatively simple situation, where a single pattern has been stored following (5) and (6). This has the following advantages: it being a simpler version of (4), it allows us to explore general features and build intuition, without as yet any serious technical subtleties, as brought up by the general model. At the same time it provides an excellent benchmark test of the general theory to which it should reduce for $J_s^{(2)} = J_\ell^{(2)} = 0$. For the remainder of this section our analysis will refer to model (5).

3.1. Solution via transfer matrices

In calculating the asymptotic free energy per neuron f it is advantageous to separate terms induced by the long-range synapses from those induced by the short-range ones, via insertion of $1 = \int dm\, \delta[m - \frac{1}{N}\sum_i \sigma_i]$. Upon using the integral representation of the δ-function, we then arrive at

$$f = -\lim_{N\to\infty} \frac{1}{\beta N} \log \int dm\, d\hat{m}\, e^{-\beta N \phi(m,\hat{m})}$$

with

$$\phi_{\text{seq}}(m, \hat{m}) = -im\hat{m} - m\theta - \frac{1}{2} J_\ell m^2 - \frac{1}{\beta N} \log R_{\text{seq}}(\hat{m})$$

$$\phi_{\text{par}}(m, \hat{m}) = -im\hat{m} - m\theta - \frac{1}{\beta N} \log R_{\text{par}}(m, \hat{m}).$$

The quantities R contain all complexities due to the short-range interactions in the model. They correspond to

$$R_{\text{seq}}(\hat{m}) = \sum_{\sigma \in \{-1,1\}^N} e^{-i\beta\hat{m}\sum_i \sigma_i} e^{\beta J_s \sum_i \sigma_i \sigma_{i+1}}$$

$$R_{\text{par}}(m, \hat{m}) = \sum_{\sigma \in \{-1,1\}^N} e^{-i\beta\hat{m}\sum_i \sigma_i} \prod_i \log[2\cosh[\beta J_\ell m + \beta\theta + \beta J_s(\sigma_{i+1} + \sigma_{i-1})]].$$

They can be calculated using the transfer-matrix method [18] giving

$$R_{\text{seq}}(\hat{m}) = \text{Tr}[T_{\text{seq}}^N] \qquad T_{\text{seq}} = \begin{pmatrix} e^{\beta J_s - i\beta\hat{m}} & e^{-\beta J_s} \\ e^{-\beta J_s} & e^{\beta J_s + i\beta\hat{m}} \end{pmatrix}$$

$$R_{\text{par}}(m, \hat{m}) = \text{Tr}[T_{\text{par}}^N] \qquad T_{\text{par}} = \begin{pmatrix} 2\cosh[\beta w_+]e^{-i\beta\hat{m}} & 2\cosh[\beta w_0] \\ 2\cosh[\beta w_0] & 2\cosh[\beta w_-]e^{i\beta\hat{m}} \end{pmatrix}$$

where $w_0 = J_\ell m + \theta$ and $w_\pm = w_0 \pm 2J_s$. The identity $\text{Tr}[T^N] = \lambda_+^N + \lambda_-^N$, in which $\lambda_\pm$ are the eigenvalues of the 2×2 matrix T enables us to take the limit $N \to \infty$ in our equations.

The integral over $(m, \hat{m})$ is then for $N \to \infty$ evaluated by steepest descent, and is dominated by the saddle points of the exponent ϕ. We thus arrive at the transparent result

$$f = \text{extr}\phi(m, \hat{m}) \begin{cases} \phi_{\text{seq}}(m, \hat{m}) = -\text{i}m\hat{m} - m\theta - \dfrac{1}{2}J_\ell m^2 - \dfrac{1}{\beta}\log\lambda_+^{\text{seq}} \\[2ex] \phi_{\text{par}}(m, \hat{m}) = -\text{i}m\hat{m} - m\theta - \dfrac{1}{\beta}\log\lambda_+^{\text{par}} \end{cases} \tag{7}$$

where λ_+^{seq} and λ_+^{par} are the largest eigenvalues of T_{seq} and T_{par}:

$$\lambda_+^{\text{seq}} = e^{\beta J_s}\cosh[\text{i}\beta\hat{m}] + [e^{2\beta J_s}\cosh^2[\text{i}\beta\hat{m}] - 2\sinh[2\beta J_s]]^{\frac{1}{2}}$$

$$\lambda_+^{\text{par}} = \cosh[\beta w_+]e^{-\text{i}\beta\hat{m}} + \cosh[\beta w_-]e^{\text{i}\beta\hat{m}} + [\cosh^2[\beta w_+]e^{-2\beta\text{i}\hat{m}}$$

$$+ \cosh^2[\beta w_-]e^{2\beta\text{i}\hat{m}} - 2\cosh[\beta w_+]\cosh[\beta w_-] + 4\cosh^2[\beta w_0]]^{\frac{1}{2}}.$$

For simplicity, we will restrict ourselves to the case where $\theta = 0$; generalization of what follows to the case of arbitrary θ, by using the full form of (7), is not significantly more difficult. The expressions defining the value(s) of the order parameter m can now be obtained from the saddle point equations $\partial_m\phi(m, \hat{m}) = \partial_{\hat{m}}\phi(m, \hat{m}) = 0$. This is a straightforward differentiation task for the sequential case. For parallel, one obtains a set of coupled nonlinear equations, namely

$$m = \mathcal{F}(m, \tilde{m}) \qquad \tilde{m} = \mathcal{F}(\tilde{m}, m) \tag{8}$$

where $\tilde{m} = -\text{i}\hat{m}/J_\ell$ and $\mathcal{F}(\cdot, \cdot)$ corresponds to

$$\mathcal{F}(p, q) = \Delta(p, q)^{-1}(e^{2\beta J_s}\sinh[\beta J_\ell(p + q)] - e^{-2\beta J_s}\sinh[\beta J_\ell(p - q)])$$

$$\Delta(p, q) = [e^{2\beta J_s}\sinh^2[\beta J_\ell(p + q)] + e^{-2\beta J_s}\sinh^2[\beta J_\ell(p - q)]$$

$$+ 2\cosh^2[\beta J_\ell p] + 2\cosh^2[\beta J_\ell q]]^{\frac{1}{2}}$$

with $\Delta(p, q) = \Delta(q, p)$. We will now show that the parallel dynamics fixed-point problem (8) admits the unique solution $m = \text{sgn}[J_\ell]\tilde{m}$, by the following argument:

For $J_\ell \geqslant 0$: $\quad m = \tilde{m} \quad$ since $0 \leqslant (m - \tilde{m})^2 = \Omega(m, \tilde{m})(m - \tilde{m})\sinh[\beta J_\ell(\tilde{m} - m)] \leqslant 0$

For $J_\ell < 0$: $\quad m = -\tilde{m} \quad$ since $0 \leqslant (m + \tilde{m})^2 = \Omega(m, \tilde{m})(m + \tilde{m})\sinh[\beta J_\ell(\tilde{m} + m)] \leqslant 0.$

where $\Omega(m, \tilde{m}) \equiv 2e^{-2\beta J_s}\Delta(m, \tilde{m})^{-1} > 0$.

Insertion of these solutions to the original function $\mathcal{F}(\cdot, \cdot)$ allows us to reduce (8) to a simple 1D fixed-point problem, similar in structure with what follows from the sequential case, namely

$$\begin{array}{llll} \text{sequential:} & \hat{m} = \text{i}mJ_\ell & m = G(m; J_\ell, J_s) & \\ \text{parallel:} & \hat{m} = \text{i}mJ_\ell & m = G(m; J_\ell, J_s) & \text{for} \quad J_\ell \geqslant 0 \\ & \hat{m} = -\text{i}mJ_\ell & m = G(m; -J_\ell, -J_s) & \text{for} \quad J_\ell < 0 \end{array} \tag{9}$$

with

$$G(m; J_\ell, J_s) = \frac{\sinh[\beta J_\ell m]}{\sqrt{\sinh^2[\beta J_\ell m] + e^{-4\beta J_s}}}. \tag{10}$$

The macroscopic observable a is generated by differentiating the reduced free energy per neuron (7):

$$\begin{array}{llll} \text{sequential:} & \hat{m} = \text{i}mJ_\ell & a = F(m; J_\ell, J_s) & \\ \text{parallel:} & \hat{m} = \text{i}mJ_\ell & a = F(m; J_\ell, J_s) & \text{for} \quad J_\ell \geqslant 0 \\ & \hat{m} = -\text{i}mJ_\ell & a = F(m; -J_\ell, -J_s) & \text{for} \quad J_\ell < 0 \end{array} \tag{11}$$

with

$$F(m; J_\ell, J_s) = \frac{\cosh[\beta J_\ell m]\sqrt{\sinh^2[\beta J_\ell m] + e^{-4\beta J_s}} + \sinh^2[\beta J_\ell m] - e^{-4\beta J_s}}{\cosh[\beta J_\ell m]\sqrt{\sinh^2[\beta J_\ell m] + e^{-4\beta J_s}} + \sinh^2[\beta J_\ell m] + e^{-4\beta J_s}}. \quad (12)$$

Note that in the absence of short-range interactions we recover the familiar Curie–Weiss law $m = \tanh[\beta J_\ell m]$ whereas in the absence of long-range interactions (9) and (11) reduce to $m = 0$ and $a = \tanh[\beta J_s]$, as they should. Finally, it is worth noting that equations (9)–(12) allow us to derive the physical properties of the parallel dynamics model from those of the sequential dynamics model via simple parameter transformations.

3.2. Phase transitions and phase diagrams

Our main order parameter m is to be solved from an equation of the form $m = G(m)$, in which $G(m) = G(m; J_\ell, J_s)$ for both sequential and parallel dynamics with $J_\ell \geqslant 0$, whereas $G(m) = G(m; -J_\ell, -J_s)$ for parallel dynamics with $J_\ell < 0$. Note that, due to $G(0; J_\ell, J_s) = 0$, the trivial solution $m = 0$ always exists. In order to obtain a phase diagram we have to perform a bifurcation analysis of the equations (9), (10), and determine the combinations of parameter values for which specific non-zero solutions are created or annihilated (the transition lines). Bifurcations of non-zero solutions occur when simultaneously $m = G(m)$ (saddle point requirement) and $1 = \partial_m G(m)$ (m is in the process of being created/annihilated). Analytical expressions for the lines in the $(\beta J_s, \beta J_\ell)$ plane where second-order transitions occur between recall states (where $m \neq 0$) and non-recall states (where $m = 0$) are obtained by solving the coupled equations $m = G(m)$ and $1 = \partial_m G(m)$ for $m = 0$. This gives

$$\text{cont trans:} \quad \begin{matrix} \text{sequential:} & \beta J_\ell = e^{-2\beta J_s} \\ \\ \text{parallel:} & \beta J_\ell = e^{-2\beta J_s} \quad \text{and} \quad \beta J_\ell = -e^{2\beta J_s} \end{matrix} \quad (13)$$

whereas for the macroscopic observable a we obtain

$$\text{sequential/parallel:} \quad a = \tanh[\beta J_s].$$

If along the lines (13) we inspect the behaviour of $G(m)$ close to $m = 0$ we can anticipate the possible existence of first-order transitions, using the properties of $G(m)$ for $m \to \pm\infty$, in combination with $G(-m) = -G(m)$. Precisely *at* the lines (13) we have $G(m) = m + \frac{1}{6}G'''(0) \cdot m^3 + \mathcal{O}(m^5)$. Since $\lim_{m\to\infty} G(m) = 1$ one knows that, when $G'''(0) > 0$, a discontinuous transition must have already taken place earlier, and that away from the lines (13) there will consequently be regions where one finds five solutions of $m = G(m)$ (two positive ones, two negative ones and $m = 0$). Along the lines (13) the condition $G'''(0) > 0$ translates into

$$\begin{matrix} \text{sequential:} & \beta J_\ell > \sqrt{3} & \text{and} & \beta J_s < -\frac{1}{4}\log 3 \\ \text{parallel:} & |\beta J_\ell| > \sqrt{3} & \text{and} & |\beta J_s| < -\frac{1}{4}\log 3. \end{matrix} \quad (14)$$

In the present models it turns out that one can also find an analytical expression for the discontinuous transition lines in the $(\beta J_s, \beta J_\ell)$ plane, in the form of a parametrization. For sequential dynamics one finds a single line, parametrized by $x = \beta J_\ell m \in [0, \infty)$:

$$\text{discont trans:} \quad \beta J_\ell(x) = \sqrt{\frac{x^3}{x - \tanh(x)}} \qquad \beta J_s(x) = -\frac{1}{4}\log\left[\frac{\tanh(x)\sinh^2(x)}{x - \tanh(x)}\right]. \quad (15)$$

This can be verified by explicit substitution into (9). Since this parametrization (15) obeys $\beta J_s(0) = -\frac{1}{4}\log 3$ and $\beta J_\ell(0) = \sqrt{3}$, the discontinuous transition indeed starts precisely at
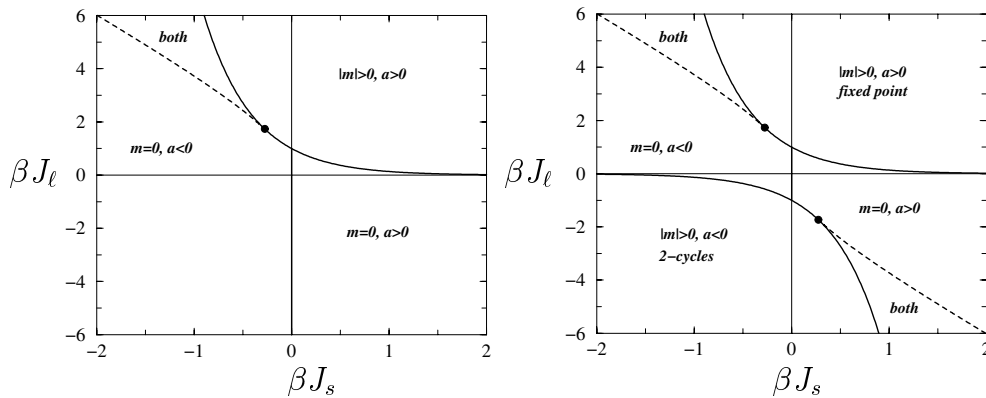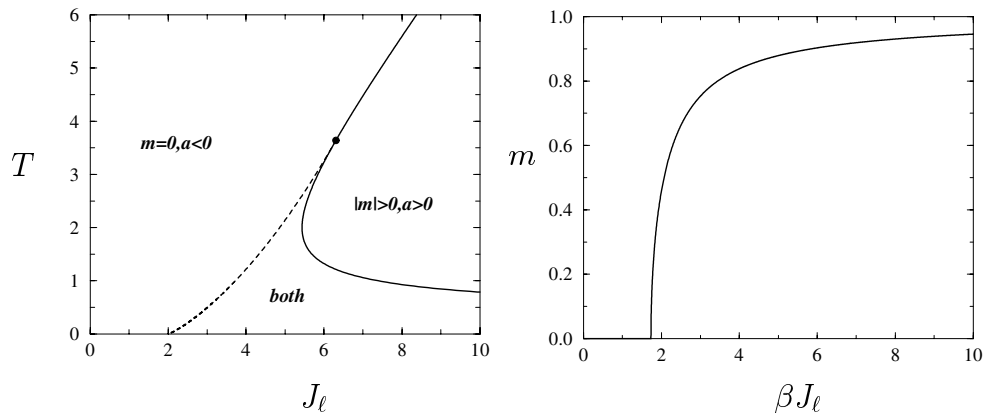
Figure 1. Left: phase diagram for sequential dynamics, involving: (i) a region with $m = 0$ only (here $a = \tanh[\beta J_s]$), (ii) a region where both the $m = 0$ state and two $m \neq 0$ states are locally stable, and (iii) a region with two locally stable $m \neq 0$ states (with opposite sign, and with identical $a > 0$). All solid curves indicate second-order transitions, whereas the dashed curves indicate first-order ones. Right: phase diagram for parallel dynamics, involving the above regions and transitions, as well as a second set of transition lines (in the region $J_\ell < 0$) which are exact reflections in the origin of the first set. Here, however, the two $m \neq 0$ physical solutions describe 2-cycles rather than fixed points, and the $J_\ell < 0$ region describes simultaneous local stability of the $m = 0$ fixed point and 2-cycles.

the point predicted by the convexity of $G(m)$ at $m = 0$, see (14). In the limit $x \to \infty$ the slope of (15) approaches $\beta J_\ell(\infty)/\beta J_s(\infty) \to -2$. For sequential dynamics the line (15) gives all non-zero solutions of the bifurcation requirements $m = G(m)$ and $1 = \partial_m G(m)$. For parallel dynamics one finds, in addition to (15), a second 'mirror' transition line, generated by the transformation $\{\beta J_\ell, \beta J_s\} \mapsto \{-\beta J_\ell, -\beta J_s\}$.

Having determined the transition lines in parameter space, we can turn to the phase diagrams. Figure 1 shows the phase diagram for the two types of dynamics, in the $(\beta J_s, \beta J_\ell)$ plane (note: of the three parameters $\{\beta, J_s, J_\ell\}$ one is redundant). For sequential dynamics we find: (i) a region where $m = 0$ only, (ii) a region where the trivial as well as two non-trivial states (a positive and a negative one) are all locally stable (selection will thus be based on initial conditions) and (iii) a region where only $m \neq 0$ states are localy stable. The transitions (i) $\to$ (iii) and (ii) $\to$ (iii) are second-order ones (solid curves of figure 1) whereas the transition (i) $\to$ (ii) is first order (dashed curve). In region (i), where $m = 0$ only, one finds $a = \tanh[\beta J_s]$ whereas in regions (ii) and (iii) a is given by the full expression of (11). For parallel dynamics we find, in addition to the sequential phase transitions, a second set of 'mirror' transition lines generated by $\{\beta J_\ell, \beta J_s\} \mapsto \{-\beta J_\ell, -\beta J_s\}$. In contrast to the sequential case however, here in the region $\beta J_\ell < 0$ and $\beta J_s < 0$ where $m \neq 0$ can be a physical state (lower left corner of the phase diagram of figure 1) one finds 2-cycles between the two $m \neq 0$ (positive and negative) recall states. This can be inferred from the exact dynamical solution that is available along the line $J_s = 0$ (see, e.g., [3]), given by the deterministic map $m(t + 1) = \tanh[\beta J_\ell m(t)]$. This map gives a stable period-2 oscillation for $\beta J_\ell < -1$, of the form $m(t) = (-1)^t m^\star$, where $m^\star = \tanh[\beta|J_\ell|m^\star]$. In the 2-cycle region one has $a = \lim_{N \to \infty} \frac{1}{N} \sum_i \langle \sigma_{i+1} \tanh[\beta h_i(\sigma)] \rangle < 0$. This can be understood on the basis of the (parallel dynamics) identity $\langle \sigma_{i+1} \tanh[\beta h_i(\sigma)] \rangle = \langle \sigma_{i+1}(t)\sigma_i(t + 1) \rangle$.

We find that in contrast to models with nearest-neighbour interactions only ($J_\ell = 0$, where no pattern recall will occur), and to models with mean-field interactions only ($J_s = 0$, where pattern recall can occur), the combination of the two interaction types leads to qualitatively new

Figure 2. Left: alternative presentation of the competition region of the sequential dynamics phase diagram of figure 1. Here the system states and transitions are drawn in the (J_ℓ, T) plane $(T = \beta^{-1})$, for $J_s = -1$. Right: the magnitude of the 'jump' of the overlap m along the first-order transition line (dashed curves in figure 1), as a function of $\beta J_\ell(x)$, $x \in [0, \infty)$, see equation (15).

modes of operation, especially in the competition region, where $J_\ell > 0$ and $J_s < 0$ (Hebbian long-range synapses, combined with anti-Hebbian short-range ones). The novel features of the diagram can play a useful role: the existence of multiple locally stable states ensures that only sufficiently strong recall cues will evoke pattern recognition; the discontinuity of the transition subsequently ensures that in the latter case the recall will be of a substantial quality. In the case of parallel, similar statements can be made in the opposite region of synaptic competition, but now involving 2-cycles. Since figure 1 cannot show the zero-noise region ($\beta = T^{-1} = \infty$), we have also drawn the interesting competition region of the sequential dynamics phase diagram in the (J_ℓ, T) plane, for $J_s = -1$ (see figure 2, left panel). At $T = 0$ one finds coexistence of recall states ($m \neq 0$) and non-recall states ($m = 0$) for any $J_\ell > 0$, as soon as $J_s < 0$. In the same figure (right picture) we show the magnitude of the discontinuity in the order parameter m along the discontinuous transition line, as a function of βJ_ℓ.

Finally we show, by way of further illustration of the coexistence mechanism, the value of reduced exponent $\phi_{\text{seq}}(m)$ given in (7), evaluated upon elimination of the auxiliary order parameter $\hat{m}$: $\phi(m) \equiv \phi_{\text{seq}}(m, im J_\ell)$. The result, for the parameter choice $(\beta, J_\ell) = (2, 3)$ and for three different short-range coupling stengths (corresponding to the three phase regimes: non-zero recall, coexistence and zero recall) is given in figure 3. In the same figure we also give the sequential dynamics bifurcation diagram displaying the value(s) of the overlap m as a function of βJ_ℓ and for $\beta J_s = -0.6$ (a line crossing all three phase regimes in figure 1).

4. Solution and phase diagrams for arbitrary p

In the general case (4), where $p > 1$, the pattern variables $\{\xi_i^\mu\}$ can no longer be transformed away as in model (6); here in order to arrive at expressions for the order parameters one has to perform the disorder average of the free energy over the realization of $\{\xi_i^\mu\}$. Due to the addition of nearest neigbour interactions, however, the disorder average has become significantly more complicated than that in infinite-range models, even in the loading regime away from saturation (i.e. $\lim_{N\to\infty} p/N = 0$). Nevertheless, interpreting the pattern variables $\{\xi_i\}$ as random bonds one can perform the transfer-matrix multiplications (and thus the relevant disorder average) via a suitable adaptation of 1D random-field techniques, see e.g. [12, 13, 16]. These are based
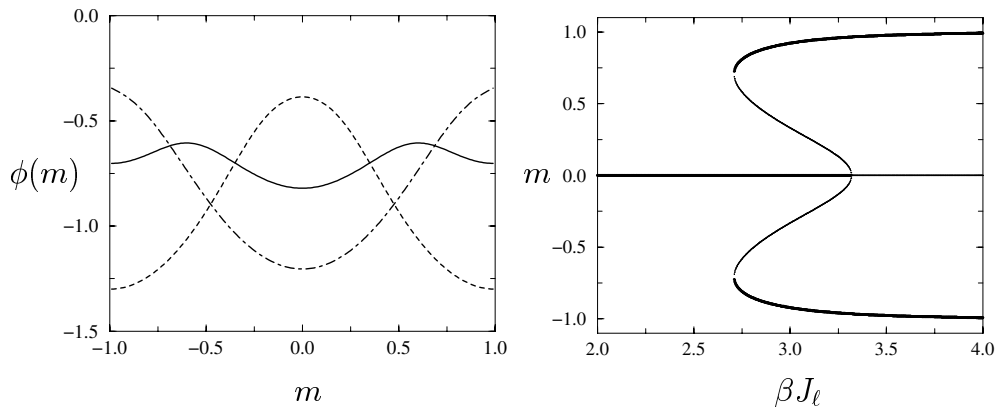
Figure 3. Left: free energy per neuron $\phi(m) = \phi_{\mathrm{seq}}(m, \mathrm{i} m J_\ell)$ as derived from equation (7) for $(\beta, J_\ell) = (2, 3)$. The three curves correspond to regimes where (i) $m \neq 0$ only (dashed curve: $J_s = -0.2$) (ii) trivial and non-trivial states are both locally stable (solid curve: $J_s = -0.8$), and (iii) $m = 0$ only (dot-dashed curve: $J_s = -1.2$). Right: sequential dynamics bifurcation diagram displaying for $\beta J_s = -0.6$ the possible recall solutions. For small βJ_ℓ, $m = 0$ is the only stable state. At a critical βJ_ℓ given by (15), m jumps to non-zero values. For increasing βJ_ℓ the unstable $m \neq 0$ solutions (thin curves) converge towards the trivial one until $\beta J_\ell = \exp(-\beta J_s)$ (here: $\beta J_\ell \approx 3.32$) where a second-order transition takes place and $m = 0$ becomes unstable.

on the derivation of a stochastic process in which observables of systems of size N are mapped to observables of systems of size $N + 1$. We will assume that in the thermodynamic limit this process leads to a unique stationary state. The free energy is then given as an integral over the distribution of a characteristic ratio of conditioned partition functions, and the order parameters follow via differentiation. We will now proceed with the solution of the general $p > 1$ case first for the less complicated sequential case (which will also serve as a guide to the technique) and then for the more involved parallel scenario.

4.1. Adaptation of RFIM techniques: sequential case

4.1.1. Disorder averaging and the free energy. We introduce the notation $m^\star = (m_0, m)$, $\hat{m}^\star = (\hat{m}_0, \hat{m})$, $\xi^\star = (\xi^0, \xi)$ where $\xi^0 = 1$. We separate the overlap order parameter via insertion of $1 = \int \mathrm{d}m^\star \, \delta[m^\star - 1/N \sum_i \sigma_i \xi_i^\star]$, and after replacing the δ-functions by their integral representation we obtain

$$f = -\lim_{N \to \infty} \frac{1}{\beta N} \log \int \mathrm{d}m^\star \, \mathrm{d}\hat{m}^\star \mathrm{e}^{-\beta N \phi_N(m^\star, \hat{m}^\star)}$$

where

$$\phi_N(m^\star, \hat{m}^\star) = -\mathrm{i} m^\star \cdot \hat{m}^\star - m_0 \theta - \frac{1}{2} J_\ell^{(1)} m_0^2 - \frac{1}{2} J_\ell^{(2)} m^2 - \frac{1}{\beta N} \log R_N(\hat{m}^\star). \tag{16}$$

The quantity $R_N(m^\star, \hat{m}^\star)$ contains as in model (5) in section 3, the summation over $\sigma = (\sigma_1, \ldots, \sigma_N)$ and the short-range neuron interactions

$$R_N(\hat{m}) = \sum_{\sigma \in \{-1, 1\}^N} \mathrm{e}^{-\mathrm{i}\beta \sum_i \sigma_i \hat{m}^\star \cdot \xi_i^\star} \mathrm{e}^{\beta \sum_i \sigma_i J_{i,i+1}^s \sigma_{i+1}} \qquad J_{i,i+1}^s \equiv J_s^{(1)} + J_s^{(2)} \xi_i \cdot \xi_{i+1}. \tag{17}$$

Due to the appearance of the random variables $\{\xi\}$ in the partition sum above one can no longer perform the transfer matrix multiplications in a trivial manner as in the $p = 1$ case.

To evaluate (17) we will first separate R_N into two different constituent parts, defined by conditioning the state of the last neuron in the chain

$$\begin{bmatrix} R_{N,\uparrow} \\ R_{N,\downarrow} \end{bmatrix} = \sum_\sigma \mathrm{e}^{-\mathrm{i}\beta \sum_i \sigma_i \hat{m}^\star \cdot \xi_i^\star} \mathrm{e}^{\beta \sum_i \sigma_i J^s_{i,i+1}\sigma_{i+1}} \begin{bmatrix} \delta_{\sigma_N,1} \\ \delta_{\sigma_N,-1} \end{bmatrix} \tag{18}$$

with

$$R_N = R_{N,\uparrow} + R_{N,\downarrow}. \tag{19}$$

We now add an extra neuron to the chain. After some simple bookkeeping and assuming non-periodic boundary conditions we derive the following recurrence relations:

$$\begin{pmatrix} R_{N+1,\uparrow} \\ R_{N+1,\downarrow} \end{pmatrix} = \begin{pmatrix} \mathrm{e}^{\beta(J^s_{N,N+1}-\mathrm{i}\hat{m}^\star \cdot \xi^\star_{N+1})} & \mathrm{e}^{-\beta(J^s_{N,N+1}+\mathrm{i}\hat{m}^\star \cdot \xi^\star_{N+1})} \\ \mathrm{e}^{-\beta(J^s_{N,N+1}-\mathrm{i}\hat{m}^\star \cdot \xi^\star_{N+1})} & \mathrm{e}^{\beta(J^s_{N,N+1}+\mathrm{i}\hat{m}^\star \cdot \xi^\star_{N+1})} \end{pmatrix} \begin{pmatrix} R_{N,\uparrow} \\ R_{N,\downarrow} \end{pmatrix}. \tag{20}$$

The recurrence matrix relation (20) will form the basis for evaluating the free energy per neuron, which will allow us to conviniently perform the partition sum in (17). In the spirit of [12, 13] we define the ratio between the conditioned quantities (18) and study their stochastic 'evolution' generated by adding new neurons successively to the chain

$$k_{j+1} = \mathrm{e}^{-2\beta \mathrm{i}\hat{m}^\star \cdot \xi^\star_{j+1}} \frac{R_{j+1,\downarrow}}{R_{j+1,\uparrow}}. \tag{21}$$

Due to their dependence on the random variables $\{\xi\}$ the above quantities $\{k_j\}$ are stochastic variables. Insertion of (20) into the above relations produces the 1D stochastic map

$$k_{i+1} = \psi(k_j; \xi_j \cdot \xi_{j+1}, \hat{m}^\star \cdot \xi^\star_j | \forall j \leqslant i)$$

$$= \frac{\mathrm{e}^{-\beta J^s_{i,i+1}} + k_i \mathrm{e}^{2\beta \mathrm{i}\hat{m}^\star \cdot \xi^\star_i} \mathrm{e}^{\beta J^s_{i,i+1}}}{\mathrm{e}^{\beta J^s_{i,i+1}} + k_i \mathrm{e}^{2\beta \mathrm{i}\hat{m}^\star \cdot \xi^\star_i} \mathrm{e}^{-\beta J^s_{i,i+1}}}. \tag{22}$$

One can now express the non-trivial part of the free energy in terms of the above ratios k_i by first using (19):

$$-\frac{1}{\beta N}\log R_N = -\frac{1}{\beta N}\log R_{N,\uparrow} + \mathcal{O}\left(\frac{1}{N}\right).$$

Upon also using (21) and (22) iteratively, in order to map the quantities $\{R_{j,\uparrow}\}$ onto $\{R_{j-1,\uparrow}\}$ (for all $j \leqslant N$), one can write the above expressions in the form

$$-\frac{1}{\beta N}\log R_{N,\uparrow}(m^\star) = -\frac{1}{\beta N}\sum_i \log[\mathrm{e}^{\beta J^s_{i,i+1}} + \mathrm{e}^{-\beta J^s_{i,i+1}}\mathrm{e}^{2\beta \mathrm{i}\hat{m}^\star \cdot \xi^\star_i}k_i]$$

$$+\frac{1}{N}\sum_i \mathrm{i}\hat{m}^\star \cdot \xi^\star_{i+1} + \mathcal{O}\left(\frac{1}{N}\right). \tag{23}$$

For $N \to \infty$ the above expressions are self-averaging and the boundary terms vanish, giving

$$-\lim_{N\to\infty}\frac{1}{\beta N}\log R_N(\hat{m}^\star) = \mathrm{i}\langle\hat{m}^\star \cdot \xi^\star\rangle_\xi - \frac{1}{\beta}\sum_{\xi'\xi}\int \mathrm{d}k'\, P(k',\xi',\xi)$$

$$\times \log[\mathrm{e}^{\beta(J^{(1)}_s + J^{(2)}_s \xi' \cdot \xi)} + \mathrm{e}^{\beta(J^{(1)}_s + J^{(2)}_s \xi' \cdot \xi)}\mathrm{e}^{2\beta \mathrm{i}\hat{m}^\star \cdot \xi^{\star\prime}}k'] \tag{24}$$

in which the probability distribution $P(\cdots)$ is defined as follows:

$$P(k',\xi',\xi) = \lim_{N\to\infty}\frac{1}{N}\sum_i \langle\delta[k'-k_i]\delta[\xi'-\xi_i]\delta[\xi-\xi_{i+1}]\rangle_{\mathrm{eq}}$$

$$= \frac{1}{2^p}P(k',\xi'). \tag{25}$$

In order to arrive at factorization of the joint probability distributions we have used the fact that, due to the form of the stochastic map (22), the quantities $\{k_j\}$ are independent of $\{\boldsymbol{\xi}_{j+1}\}$, i.e. of the pattern variables at the next site. The dependence on $\{\boldsymbol{\xi}_j\}$, however, does not allow us to write down immediately (22) in terms of a Markov process. We thus introduce the auxiliary variables $\{\boldsymbol{\lambda}_j\}$, so that $\{\boldsymbol{\xi}_j\}$ itself becomes one of the stochastically evolving variables, and the extended process becomes indeed Markovian:

$$\begin{pmatrix} k \\ \boldsymbol{\lambda} \end{pmatrix}_{i+1} = \Psi \left[\begin{pmatrix} k \\ \boldsymbol{\lambda} \end{pmatrix}_i ; \boldsymbol{\xi}_{i+1} \right] = \begin{pmatrix} \psi(k_i; \boldsymbol{\lambda}_i \cdot \boldsymbol{\xi}_{i+1}, \hat{m}^\star \cdot \boldsymbol{\lambda}_i^\star) \\ \boldsymbol{\xi}_{i+1} \end{pmatrix}.$$

Equivalently

$$P_{i+1}(k, \boldsymbol{\lambda}) = \frac{1}{2^p} \sum_{\boldsymbol{\lambda}'} \int \mathrm{d}k' \, W \left[\begin{pmatrix} k' \\ \boldsymbol{\lambda}' \end{pmatrix} \rightarrow \begin{pmatrix} k \\ \boldsymbol{\lambda} \end{pmatrix} \right] P_i(k', \boldsymbol{\lambda}') \tag{26}$$

where for the transition probabilities $W[\cdots]$ we define

$$W \left[\begin{pmatrix} k' \\ \boldsymbol{\lambda}' \end{pmatrix} \rightarrow \begin{pmatrix} k \\ \boldsymbol{\lambda} \end{pmatrix} \right] = \langle \delta_{\boldsymbol{\xi}, \boldsymbol{\lambda}} \delta[k - \psi_{\text{seq}}(k', \boldsymbol{\lambda}' \cdot \boldsymbol{\xi}, \hat{m}^\star \cdot \boldsymbol{\lambda}^{\star'})] \rangle_{\boldsymbol{\xi}}.$$

The evaluation of the non-trivial part of the free energies (24) has now been reduced to determining the (stationary) distribution of (26), which will be denoted by $P_\infty(k)$. To achieve this final objective we follow [12, 13] and introduce the integrated densities $\hat{P}(k) = \int_0^k \mathrm{d}z \, P(z)$. After some algebra to eliminate the δ-functions of the transition probabilities via the identity $\int \mathrm{d}x \, \delta[g(x)] f(x) = f(g^{\text{inv}}(0))/|\partial_x g(0)|$, we then obtain the following recursive relation:

$$\hat{P}_{i+1}(k, \boldsymbol{\lambda}) = \frac{1}{2^p} \sum_{\boldsymbol{\lambda}'} \hat{P}_i(B(k; \boldsymbol{\lambda}' \cdot \boldsymbol{\lambda}, \hat{m}^\star \cdot \boldsymbol{\lambda}^{\star'}), \boldsymbol{\lambda}') \tag{27}$$

where the function $B(k)$ corresponds to

$$B(k) = \frac{k \mathrm{e}^{\beta(J_s^{(1)} + J_s^{(2)} \boldsymbol{\lambda}' \cdot \boldsymbol{\lambda})} - \mathrm{e}^{-\beta(J_s^{(1)} + J_s^{(2)} \boldsymbol{\lambda}' \cdot \boldsymbol{\lambda})}}{\mathrm{e}^{\beta(J_s^{(1)} + J_s^{(2)} \boldsymbol{\lambda}' \cdot \boldsymbol{\lambda})} - k \mathrm{e}^{-\beta(J_s^{(1)} + J_s^{(2)} \boldsymbol{\lambda}' \cdot \boldsymbol{\lambda})}} \mathrm{e}^{-2\beta \mathrm{i} \hat{m}^\star \cdot \boldsymbol{\lambda}^{\star'}}. \tag{28}$$

We have thus derived as yet fully exact expressions for the disorder-averaged free energy (24), as integral over the distribution of the stochastic quantity $\{k\}$, which can be evaluated by numerical iteration of the recursive relation (27).

4.1.2. The 'pure state' ansatz and symmetries of the model. We will now look for the so-called 'pure-state' solutions: we will assume that for $N \rightarrow \infty$ there is only one component m_μ of order $\mathcal{O}(1)$ (for simplicity we will take $\mu = 1$) whereas for all $\mu > 1$ m_μ is of order $\mathcal{O}(N^{-\frac{1}{2}})$: $m^\star = (m_0, m, 0, \ldots, 0)$ and $\hat{m}^\star = (\hat{m}_0, \hat{m}, 0, \ldots, 0)$. This is the standard ansatz made in (infinite-range) associative memory models, which gives the dominant states of the system. The fact that this is also true for the present type of models is supported by numerical simulations, see section 6. Using this simplification we will now prove that the stationary integrated density $\hat{P}_\infty(\cdots)$ is independent of all non-condensed pattern components. This will be shown by induction. We will show that if $\hat{P}_i(k, \boldsymbol{\lambda})$ is independent of λ_μ for some $\mu > 1$, then $\hat{P}_{i+1}(k, \boldsymbol{\lambda})$ will also be independent of λ_μ. This will then immediately imply that if the densities are independent of $\{\lambda_\mu\}$ for all $\mu > 1$ at step i of the process (27), this will remain so for all $\mu > 1$ at any step $j > i$. Usage of the spin-flip operator $F_\mu x = (x_1, \ldots, -x_\mu, \ldots, x_p)$ allows us to write

$$\Delta_{i+1} = \hat{P}_{i+1}(k, F_\mu \boldsymbol{\lambda}) - \hat{P}_{i+1}(k, \boldsymbol{\lambda})$$

$$= \frac{1}{2^p} \sum_{\boldsymbol{\lambda}'} \{\hat{P}_i(B(k; \boldsymbol{\lambda}' \cdot \boldsymbol{\lambda}, \hat{m}_0 + \hat{m}\lambda'), F_\mu \boldsymbol{\lambda}') - \hat{P}_i(B(k; \boldsymbol{\lambda}' \cdot \boldsymbol{\lambda}, \hat{m}_0 + \hat{m}\lambda'), \boldsymbol{\lambda}')\}.$$

If at step i the identity $\Delta_i = 0$ is true, then $\hat{P}_i(B(k), F_\mu \boldsymbol{\lambda}) = \hat{P}_i(B(k), \boldsymbol{\lambda})$ and thus $\Delta_{i+1} = 0$. Upon choosing suitable initial conditions we can thus construct equilibrium integrated densities with the stated property; combination with the assumed ergodicity of the process then implies that the unique solution must have the property. This completes the proof. We can consequently write the stationary integrated densities in the form: $\hat{P}_\infty(k, \lambda)$, where $\lambda \in \{-1, 1\}$ corresponds to the condensed pattern component

$$\hat{P}_{i+1}(k, \lambda) = \tfrac{1}{2} \sum_{\lambda'=\pm1} \hat{P}_i(B(k; \lambda'\lambda, \hat{m}_0 + \hat{m}\lambda'), \lambda') \tag{29}$$

where $B(k)$ is given by (28). One can also exploit the fact that the pattern variables $\{\boldsymbol{\lambda}\}$ appear in inner-products only, to simplify the non-trivial integrated expressions of equation (24). Since the argumentation will be qualitative we will forget about the details of these expressions and we will denote the integrated logarithmic expressions simply by

$$\Phi(\boldsymbol{\lambda}' \cdot \boldsymbol{\lambda}) = \log[\mathrm{e}^{\beta(J_s^{(1)}+J_s^{(2)}\boldsymbol{\lambda}\cdot\boldsymbol{\lambda}')} + \mathrm{e}^{-\beta(J_s^{(1)}+J_s^{(2)}\boldsymbol{\lambda}\cdot\boldsymbol{\lambda}')} + k'\mathrm{e}^{2\beta\mathrm{i}(\hat{m}_0+\hat{m}\boldsymbol{\lambda}')}].$$

Upon using the gauge transformation $\lambda_\mu = \tau_\mu \lambda'_\mu$ where τ_μ are auxiliary Ising variables, the non-trivial parts of expressions (24)—corresponding to the integrals over the stochastic variables $\{k_j\}$ after the distribution factorization (25) and the 'pure state' ansatz—take the form

$$\frac{1}{2^p} \sum_{\boldsymbol{\lambda}'} \sum_{\boldsymbol{\lambda}} \int \mathrm{d}k' \, P_\infty^s(k', \boldsymbol{\lambda}') \Phi(\boldsymbol{\lambda}' \cdot \boldsymbol{\lambda}; k', \hat{m}_0 + \hat{m}\boldsymbol{\lambda}')$$

$$= \frac{2^{p-1}}{2^p} \sum_{\boldsymbol{\lambda}'} \sum_{\tau} \int \mathrm{d}k' \, P_\infty^s(k', \boldsymbol{\lambda}') \Phi\left(\sum_{\mu=1}^p \tau_\mu; k', \hat{m}_0 + \hat{m}\boldsymbol{\lambda}'\right)$$

$$= \tfrac{1}{2} \sum_{\lambda'=\pm1} \sum_{\mathcal{N}_\tau=0}^p \int \mathrm{d}k' \binom{p}{\mathcal{N}_\tau} P_\infty^s(k', \boldsymbol{\lambda}') \Phi(2\mathcal{N}_\tau - p; k', \hat{m}_0 + \hat{m}\boldsymbol{\lambda}')$$

where $\mathcal{N}_\tau$ represents the number of neurons with states equal to $+1$ in the configuration of τ. We have thus replaced all summations over the 2^p configurations of the vectors $\{\boldsymbol{\lambda}, \boldsymbol{\lambda}'\}$ and by summations over binary- and p-state variables.

4.2. Adaptation of RFIM techniques: parallel case

4.2.1. Disorder averaging and the free energy. The analysis of the parallel dynamics model follows closely the sequential one. We start by introducing the notation $\boldsymbol{m}^\star = (m_0, \boldsymbol{m})$, $\hat{\boldsymbol{m}}^\star = (\hat{m}_0, \hat{\boldsymbol{m}})$, $\boldsymbol{\xi}^\star = (\xi^0, \boldsymbol{\xi})$ where $\xi^0 = 1$ in the expression for the free energy per neuron. As before, we separate the overlap order parameter via insertion of $1 = \int \mathrm{d}\boldsymbol{m}^\star \delta[\boldsymbol{m}^\star - 1/N \sum_i \sigma_i \boldsymbol{\xi}_i^\star]$, and we replace the δ-functions by their integral representation giving

$$f = -\lim_{N\to\infty} \frac{1}{\beta N} \log \int \mathrm{d}\boldsymbol{m}^\star \, \mathrm{d}\hat{\boldsymbol{m}}^\star \mathrm{e}^{-\beta N \phi_N(\boldsymbol{m}^\star, \hat{\boldsymbol{m}}^\star)}$$

$$\phi_N(\boldsymbol{m}^\star, \hat{\boldsymbol{m}}^\star) = -\mathrm{i}\boldsymbol{m}^\star \cdot \hat{\boldsymbol{m}}^\star - m_0\theta - \frac{1}{\beta N} \log R_N(\boldsymbol{m}^\star, \hat{\boldsymbol{m}}^\star) \tag{30}$$

with

$$R_N(\boldsymbol{m}^\star, \hat{\boldsymbol{m}}^\star) = \sum_{\sigma\in\{-1,1\}^N} \mathrm{e}^{-\mathrm{i}\beta \sum_i \sigma_i \hat{\boldsymbol{m}}^\star \cdot \boldsymbol{\xi}_i^\star} \prod_i \log[2\cosh[\beta(J_i^\ell + \sigma_{i-1}J_{i-1,i}^s + \sigma_{i+1}J_{i,i+1}^s)]] \tag{31}$$

where the short-hands $J_{i,i+1}^s$ and J_i^ℓ correspond to

$$J_{i,i+1}^s = J_s^{(1)} + J_s^{(2)}\boldsymbol{\xi}_i \cdot \boldsymbol{\xi}_{i+1} \qquad J_i^\ell = \theta + J_\ell^{(1)}m_0 + J_\ell^{(2)}\boldsymbol{\xi}_i \cdot \boldsymbol{m}.$$

As in the sequential case we now aim to derive a recurrence relation between conditioned quantities which follow from R_N and which will allow us to perform the partition sum and express observable quantities in terms of simple stochastic variables. It appears that this can be achieved here by conditioning the quantity R_N on the states of the last *two* spins of the chain producing the following four quantities:

$$
\begin{bmatrix} R_{N,\uparrow\uparrow} \\ R_{N,\uparrow\downarrow} \\ R_{N,\downarrow\uparrow} \\ R_{N,\downarrow\downarrow} \end{bmatrix} = \sum_\sigma e^{-i\beta \sum_i \sigma_i \hat{m}^\star \cdot \xi_i^\star} e^{\sum_i \log[2\cosh[\beta(J_i^\ell + \sigma_{i-1} J_{i-1,i}^s + \sigma_{i+1} J_{i,i+1}^s)]]} \begin{bmatrix} \delta_{\sigma_{N-1},1}\delta_{\sigma_N,1} \\ \delta_{\sigma_{N-1},1}\delta_{\sigma_N,-1} \\ \delta_{\sigma_{N-1},-1}\delta_{\sigma_N,1} \\ \delta_{\sigma_{N-1},-1}\delta_{\sigma_N,-1} \end{bmatrix}. \tag{32}
$$

We now add an extra neuron to the chain. Assuming non-periodic boundary conditions we derive the matrix relations

$$
\begin{pmatrix} R_{N+1,\uparrow\uparrow} \\ R_{N+1,\uparrow\downarrow} \end{pmatrix} = 2Q_{N,N+1}^+ \begin{pmatrix} \frac{e^{-i\beta\hat{m}^\star \cdot \xi_{N+1}^\star}}{Q_{N-1,N}^+} A_{(+,+)}^{(N)} & \frac{e^{-i\beta\hat{m}^\star \cdot \xi_{N+1}^\star}}{Q_{N-1,N}^-} A_{(-,+)}^{(N)} \\ \frac{e^{i\beta\hat{m}^\star \cdot \xi_{N+1}^\star}}{Q_{N-1,N}^+} A_{(+,-)}^{(N)} & \frac{e^{i\beta\hat{m}^\star \cdot \xi_{N+1}^\star}}{Q_{N-1,N}^-} A_{(-,-)}^{(N)} \end{pmatrix} \begin{pmatrix} R_{N,\uparrow\uparrow} \\ R_{N,\downarrow\uparrow} \end{pmatrix}
$$

$$
\begin{pmatrix} R_{N+1,\downarrow\uparrow} \\ R_{N+1,\downarrow\downarrow} \end{pmatrix} = 2Q_{N,N+1}^- \begin{pmatrix} \frac{e^{-i\beta\hat{m}^\star \cdot \xi_{N+1}^\star}}{Q_{N-1,N}^+} A_{(+,+)}^{(N)} & \frac{e^{-i\beta\hat{m}^\star \cdot \xi_{N+1}^\star}}{Q_{N-1,N}^-} A_{(-,+)}^{(N)} \\ \frac{e^{i\beta\hat{m}^\star \cdot \xi_{N+1}^\star}}{Q_{N-1,N}^+} A_{(+,-)}^{(N)} & \frac{e^{i\beta\hat{m}^\star \cdot \xi_{N+1}^\star}}{Q_{N-1,N}^-} A_{(-,-)}^{(N)} \end{pmatrix} \begin{pmatrix} R_{N,\uparrow\downarrow} \\ R_{N,\downarrow\downarrow} \end{pmatrix} \tag{33}
$$

with the short-hand abbreviations

$$
A_{(\pm,\pm)}^{(n)} = A_{(\pm,\pm)}^{(n)}(\xi_{n-1} \cdot \xi_n, \xi_n \cdot \xi_{n+1}, \xi_n \cdot m) = \cosh[\beta(J_n^\ell \pm J_{n-1,n}^s \pm J_{n,n+1}^s)]
$$
$$
Q_{n,n+1}^\pm = Q^\pm(\xi_n \cdot \xi_{n+1}, \xi_n \cdot m) = \cosh[\beta(J_{n+1}^\ell \pm J_{n,n+1}^s)]. \tag{34}
$$

The fact that parallel dynamics leads to a recurrence process given by 4×4 random matrices, instead of the simpler 2×2 random matrices of the sequential case, is due to the appearance of short-range couplings of the form $\cosh[\beta(J_i^\ell + \sigma_{i-1}J_{i-1,i}^s + \sigma_{i+1}J_{i,i+1}^s)]$ in (31), rather than the more familiar exponentials. This, in turn, is an immediate consequence of the form of the pseudo-Hamiltonian (3). We also note that in the parallel case the two reduced 2×2 matrices differ only by the prefactors $Q_{N,N+1}^\pm$. The recurrence matrices (33) will now allow us to follow in the footsteps of the sequential analysis and evaluate the asymptotic free energy per neuron. We also note that adding the four new quantities (32) one recovers R_N:

$$
R_N = R_{N,\uparrow\uparrow} + R_{N,\uparrow\downarrow} + R_{N,\downarrow\uparrow} + R_{N,\downarrow\downarrow}. \tag{35}
$$

In order to evaluate the relevant partition sum we will use the ratios of the conditioned quantities (32). For that purpose we define

$$
k_{n+1}^{(1)} = e^{-2\beta i \hat{m}^\star \cdot \xi_{n+1}^\star} \frac{R_{n+1,\uparrow\downarrow}}{R_{n+1,\uparrow\uparrow}} \qquad k_{n+1}^{(2)} = e^{-2\beta i \hat{m}^\star \cdot \xi_{n+1}^\star} \frac{R_{n+1,\downarrow\downarrow}}{R_{n+1,\downarrow\uparrow}}
$$
$$
k_{n+1}^{(3)} = \frac{Q_{n,n+1}^+}{Q_{n,n+1}^-} \frac{R_{n+1,\downarrow\downarrow}}{R_{n+1,\uparrow\downarrow}}. \tag{36}
$$

As in the less involved sequential case, all the equilibrium properties of the parallel dynamics model will be dominated by the stationary distribution of these variables. Insertion of the matrix elements of (33) into (36) gives

$$
k_{n+1}^{(1)} = \frac{A_{(+,-)}^{(n)} k_n^{(2)} + A_{(-,-)}^{(n)} k_n^{(1)} k_n^{(3)}}{A_{(+,+)}^{(n)} k_n^{(2)} + A_{(-,+)}^{(n)} k_n^{(1)} k_n^{(3)}} \qquad k_{n+1}^{(2)} = \frac{A_{(+,-)}^{(n)} + A_{(-,-)}^{(n)} k_n^{(3)}}{A_{(+,+)}^{(n)} + A_{(-,+)}^{(n)} k_n^{(3)}}
$$
$$
k_{n+1}^{(3)} = \frac{A_{(+,-)}^{(n)} k_n^{(1)} k_n^{(2)} + A_{(-,-)}^{(n)} k_n^{(1)} k_n^{(2)} k_n^{(3)}}{A_{(+,-)}^{(n)} k_n^{(2)} + A_{(-,-)}^{(n)} k_n^{(1)} k_n^{(3)}} e^{2\beta i \hat{m}^\star \cdot \xi_n^\star}. \tag{37}
$$

The above stochastic mappings turn out to be greatly simplified: we observe that, if the identity $k_n^{(1)} = k_n^{(2)}$ is true, then also $k_{n+1}^{(1)} = k_{n+1}^{(2)}$. Furthermore, it can be easily checked that this is

the case for $n = 2$. We are thus guaranteed that $k_n^{(1)} = k_n^{(2)}$ for all $n \geqslant 2$, and now all three quantities $\{k_n^{(1)}, k_n^{(2)}, k_n^{(3)}\}$ can be expressed (for any $n \geqslant 2$) in terms of a single stochastic variable which we will take to be $k_n^{(1)} \equiv k_n$:

$$k_{n+1}^{(1)} = k_{n+1} \qquad k_{n+1}^{(2)} = \frac{A_{(+,-)}^{(n)} + A_{(-,-)}^{(n)} k_{n-1} e^{2\beta i \hat{m}^\star \cdot \xi^\star}}{A_{(+,+)}^{(n)} + A_{(-,+)}^{(n)} k_{n-1} e^{2\beta i \hat{m}^\star \cdot \xi^\star}} \qquad k_{n+1}^{(3)} = k_n e^{2\beta i \hat{m}^\star \cdot \xi_n^\star}. \tag{38}$$

Therefore, the parallel dynamics problem can be described as the sequential one by a single stochastic process

$$\begin{aligned}
k_{i+1} &= \psi(k_{j-1}; \xi_{j-1} \cdot \xi_j, \xi_j \cdot \xi_{j+1}, m \cdot \xi_j, \hat{m}^\star \cdot \xi_{j-1}^\star | \forall j \leqslant i) \\
&= (\cosh[\beta(J_i^\ell + J_{i-1,i}^s - J_{i,i+1}^s)] \\
&\quad + e^{2\beta i \hat{m}^\star \cdot \xi_{i-1}^\star} k_{i-1} \cosh[\beta(J_i^\ell - J_{i-1,i}^s - J_{i,i+1}^s)]) \\
&\quad \times \{\cosh[\beta(J_i^\ell + J_{i-1,i}^s + J_{i,i+1}^s)] \\
&\quad + e^{2\beta i \hat{m}^\star \cdot \xi_{i-1}^\star} k_{i-1} \cosh[\beta(J_i^\ell - J_{i-1,i}^s + J_{i,i+1}^s)]\}^{-1}.
\end{aligned} \tag{39}$$

We note in passing that the process (39) distinguishes between even and odd sites, and produces two independent sets of stochastic variables $\{k_j\}$.

We now turn to the evaluation of the non-trivial part of the free energy (30) which we first write as

$$-\frac{1}{\beta N} \log R_N = -\frac{1}{\beta N} \log R_{N,\uparrow\uparrow} + \mathcal{O}\left(\frac{1}{N}\right).$$

Using the ratios $\{k_n^{(\ell)}; \ell = 1, 2, 3\}$ (36) iteratively to map the quantities $\{R_{n,\uparrow\uparrow}\}$ onto $\{R_{n-1,\uparrow\uparrow}\}$ (for all $n \leqslant N$) and subsequently reduce the three ratios $\{k_n^{(\ell)}\}$ to a single one via (38) one can write the above expressions in the form

$$\begin{aligned}
-\frac{1}{\beta N} \log R_{N,\uparrow\uparrow}(m^\star, \hat{m}^\star) &= -\frac{1}{\beta N} \sum_i \log[2 \cosh[\beta(J_{i+1}^\ell + J_{i,i+1}^s + J_{i+1,i+2}^s)] \\
&\quad + 2 \cosh[\beta(J_{i+1}^\ell - J_{i,i+1}^s + J_{i+1,i+2}^s)] e^{2\beta i \hat{m}^\star \cdot \xi_i^\star} k_i] \\
&\quad + \frac{1}{N} \sum_i i \hat{m}^\star \cdot \xi_{i+1}^\star - \frac{1}{\beta N} \sum_i \log[Q_{i+1,i+2}^+ / Q_{i+1,i+2}^-] + \mathcal{O}\left(\frac{1}{N}\right)
\end{aligned}$$

where the terms $Q_{j,k}^\pm$ are defined at (34). For $N \to \infty$ the above expressions self-average giving

$$\begin{aligned}
-\lim_{N\to\infty} \frac{1}{\beta N} \log R_N(m^\star, \hat{m}^\star) &= i \langle \hat{m}^\star \cdot \xi^{\star\prime} \rangle_{\xi'} - \frac{1}{\beta} \log 2 - \frac{1}{\beta} \left\langle \log\left[\frac{Q^+(\xi' \cdot \xi, \xi \cdot m)}{Q^-(\xi' \cdot \xi, \xi \cdot m)}\right]\right\rangle_{\{\xi',\xi\}} \\
&\quad - \frac{1}{\beta} \sum_{\xi'' \xi' \xi} \int dk'' \, P(k'', \xi'', \xi', \xi) \log[A_{(+,+)}(\xi'' \cdot \xi', \xi' \cdot \xi, \xi' \cdot m) \\
&\quad + A_{(-,+)}(\xi'' \cdot \xi', \xi' \cdot \xi, \xi' \cdot m) k'' e^{2\beta i \hat{m}^\star \cdot \xi^{\star\prime\prime}}]
\end{aligned} \tag{40}$$

in which the probability distribution $P(\cdots)$ is defined as the equilibrium expectation value:

$$\begin{aligned}
P(k'', \xi'', \xi', \xi) &= \lim_{N\to\infty} \frac{1}{N} \sum_i \langle \delta[k'' - k_{i-1}] \delta[\xi'' - \xi_{i-1}] \delta[\xi' - \xi_i] \delta[\xi - \xi_{i+1}] \rangle_{\text{eq}} \\
&= \frac{1}{2^{2p}} P(k'', \xi'').
\end{aligned} \tag{41}$$

Factorisation in the last step of (41) has been achieved due to the fact that the quantity $\{k_n\}$ is independent of $\{\boldsymbol{\xi}_{n+1}\}$, see (39). Nevertheless, to arrive to a Markovian process we are forced to introduce (as in the sequential case) the auxiliary variables $\{\boldsymbol{\lambda}_n\}$:

$$\begin{pmatrix} k \\ \boldsymbol{\lambda} \end{pmatrix}_{i+1} = \Psi\left[\begin{pmatrix} k \\ \boldsymbol{\lambda} \end{pmatrix}_{i-1}; \boldsymbol{\xi}_{i+1}, \boldsymbol{\xi}_i \right] = \begin{pmatrix} \psi(k_{i-1}; \boldsymbol{\lambda}_{i-1} \cdot \boldsymbol{\xi}_i, \boldsymbol{\xi}_i \cdot \boldsymbol{\xi}_{i+1}, \boldsymbol{m} \cdot \boldsymbol{\xi}_i, \hat{\boldsymbol{m}}^\star \cdot \boldsymbol{\lambda}_{i-1}^\star) \\ \boldsymbol{\xi}_{i+1} \end{pmatrix}.$$

Equivalently

$$P_{i+1}(k, \boldsymbol{\lambda}) = \frac{1}{2^p} \sum_{\boldsymbol{\lambda}''} \int \mathrm{d}k'' \, W\left[\begin{pmatrix} k'' \\ \boldsymbol{\lambda}'' \end{pmatrix} \to \begin{pmatrix} k \\ \boldsymbol{\lambda} \end{pmatrix} \right] P_i(k'', \boldsymbol{\lambda}'') \tag{42}$$

with $W[\cdots]$ defined as the probability for state $(k'', \boldsymbol{\lambda}'')$ to move into state $(k, \boldsymbol{\lambda})$ averaged over the random variables $\{\boldsymbol{\xi}, \boldsymbol{\xi}'\}$ (which control the 'path' of the states)

$$W\left[\begin{pmatrix} k'' \\ \boldsymbol{\lambda}'' \end{pmatrix} \to \begin{pmatrix} k \\ \boldsymbol{\lambda} \end{pmatrix} \right] = \langle \delta_{\boldsymbol{\xi}, \boldsymbol{\lambda}} \delta[k - \psi(k'', \boldsymbol{\lambda}'' \cdot \boldsymbol{\xi}', \boldsymbol{\xi}' \cdot \boldsymbol{\xi}, \boldsymbol{m} \cdot \boldsymbol{\xi}', \hat{\boldsymbol{m}}^\star \cdot \boldsymbol{\lambda}^{\star''})] \rangle_{\boldsymbol{\xi}\boldsymbol{\xi}'}.$$

We will assume that in the limit $i \to \infty$ the density (42) becomes stationary. Again, as in the sequential case the evaluation of the non-trivial part of the asymptotic free energy (40) has been reduced to determining the asymptotic distribution function (42), which will be denoted by $P_\infty(k)$. We introduce the integrated density $\hat{P}(k) = \int_0^k \mathrm{d}z \, P(z)$ which allows us to derive the following recursive relation:

$$\hat{P}_{i+1}(k, \boldsymbol{\lambda}) = \frac{1}{2^{2p}} \sum_{\boldsymbol{\lambda}''} \sum_{\boldsymbol{\xi}'} \hat{P}_i(B(k; \boldsymbol{\lambda}'' \cdot \boldsymbol{\xi}', \boldsymbol{\xi}' \cdot \boldsymbol{\lambda}, \boldsymbol{m} \cdot \boldsymbol{\xi}', \hat{\boldsymbol{m}}^\star \cdot \boldsymbol{\lambda}^{\star'}), \boldsymbol{\lambda}'') \tag{43}$$

where the function $B(k)$ corresponds to

$$B(k) = \frac{k A_{(+,+)} - A_{(+,-)}}{A_{(-,-)} - k A_{(-,+)}} \mathrm{e}^{-2\beta \mathrm{i} \hat{\boldsymbol{m}}^\star \cdot \boldsymbol{\lambda}^{\star''}} \tag{44}$$

with

$$\begin{aligned} A_{(\pm,\pm)} &= A_{(\pm,\pm)}(\boldsymbol{\lambda}'' \cdot \boldsymbol{\xi}', \boldsymbol{\xi}' \cdot \boldsymbol{\lambda}, \boldsymbol{m} \cdot \boldsymbol{\xi}') \\ &= \cosh[\beta(J^\ell(\boldsymbol{m} \cdot \boldsymbol{\xi}', m_0, \theta) \pm J_s(\boldsymbol{\lambda}'' \cdot \boldsymbol{\xi}') \pm J_s(\boldsymbol{\xi}' \cdot \boldsymbol{\lambda}))]. \end{aligned}$$

Equation (43) differs from the corresponding sequential one (27) by the appearance of a second summation over a 2^p-state variable. This will be simplified further in the following section. To this stage we have derived (as in the simpler sequential case) expressions for the parallel dynamics free energy (40), as integrals over the distribution of the stochastic quantity $\{k\}$ which can be evaluated by numerical iteration of (43).

4.2.2. The 'pure state' ansatz and symmetries of the model. We will now restrict ourselves to the 'pure-state' solutions: $\boldsymbol{m}^\star = (m_0, m, 0, \dots, 0)$ and $\hat{\boldsymbol{m}}^\star = (\hat{m}_0, \hat{m}, 0, \dots, 0)$. Following this ansatz we will also prove by induction that the stationary integrated density $\hat{P}_\infty(\cdots)$ (43) is independent of all non-condensed pattern components, based on the same line of reasoning as in the sequential case: we will show that the difference between two integrated densities which differ by having their μth pattern variable flipped remains zero:

$$\begin{aligned} \Delta_{i+1} &= \hat{P}_{i+1}(k, F_\mu \boldsymbol{\lambda}) - \hat{P}_{i+1}(k, \boldsymbol{\lambda}) \\ &= \frac{1}{2^{2p}} \sum_{\boldsymbol{\lambda}'', \boldsymbol{\xi}'} \{\hat{P}_i(B(k; \boldsymbol{\lambda}'' \cdot \boldsymbol{\xi}', \boldsymbol{\xi}' \cdot \boldsymbol{\lambda}, m_0 + m\xi', \hat{m}_0 + \hat{m}\lambda''), F_\mu \boldsymbol{\lambda}') \\ &\quad - \hat{P}_i(B(k; \boldsymbol{\lambda}'' \cdot \boldsymbol{\xi}', \boldsymbol{\xi}' \cdot \boldsymbol{\lambda}, m_0 + m\xi', \hat{m}_0 + \hat{m}\lambda''), \boldsymbol{\lambda}')\}. \end{aligned}$$

If at step i the identity $\Delta_i = 0$ is true, then $\hat{P}_i(B(k), F_\mu \boldsymbol{\lambda}) = \hat{P}_i(B(k), \boldsymbol{\lambda})$ and thus $\Delta_{i+1} = 0$. This identity now implies that if the density $\hat{P}_i(k, \boldsymbol{\lambda})$ is independent of all $\{\lambda_\mu; \mu > 1\}$ at

step i of the recurrence process (43), this will remain the case for all steps $j > i$. We can therefore construct densities with appropriate initial conditions which together with the assumed ergodicity implies that the unique stationary solution must have the stated property. We can consequently simplify our notation and drop all non-condensed pattern components (since they are shown to be completely irrelevant) and write (43) in the simple form

$$\hat{P}_{i+1}(k, \lambda) = \tfrac{1}{4} \sum_{\lambda''=\pm 1} \sum_{\xi'=\pm 1} \hat{P}_i(B(k; \lambda''\xi', \xi'\lambda, m_0 + m\xi', \hat{m}_0 + \hat{m}\lambda''), \lambda'') \quad (45)$$

where the function $B(k)$ is given by (44). Finally, it turns out that one can again simplify the summations over the 2^p configurations of the various vector variables appearing in (40) and replace them by summations over binary and p-state variables. We denote the integrated logarithmic expressions of (40) by

$$\Phi(\lambda'' \cdot \xi', \xi' \cdot \lambda) = \log[A_{(+,+)}(\lambda'' \cdot \xi', \xi' \cdot \lambda, \xi'm)$$
$$+ A_{(-,+)}(\lambda'' \cdot \xi', \xi' \cdot \lambda, \xi'm)k''e^{2\beta i(\hat{m}_0 + \hat{m}\lambda'')}].$$

Using the gauge transformations $\lambda''_\mu = \tau_\mu \xi'_\mu$ and $\lambda_\mu = \eta_\mu \xi'_\mu$, where $\tau_\mu, v_\mu \in \{-1, 1\}$, the non-trivial part of (40) takes the form

$$\frac{1}{2^{2p}} \sum_{\lambda''} \sum_{\xi'} \sum_{\lambda} \int dk'' \, P_\infty(k'', \lambda'') \Phi(\lambda'' \cdot \xi', \xi' \cdot \lambda, m\xi'; k'', \hat{m}_0 + \hat{m}\lambda'')$$

$$= \frac{2^{p-1}}{2^{2p}} \sum_{\tau} \sum_{\xi'} \sum_{\eta} \int dk'' \, P_\infty(k'', \tau_1\xi')$$

$$\times \Phi\left(\tau_1 + \sum_{\mu=2}^{p} \tau_\mu, \sum_{\mu=1}^{p} \eta_\mu, m\xi'; k'', \hat{m}_0 + \hat{m}\tau_1\xi'\right)$$

$$= \tfrac{1}{4} \sum_{\tau_1=\pm 1} \sum_{\xi'=\pm 1} \sum_{\mathcal{N}_\tau=0}^{p-1} \sum_{\mathcal{N}_\eta=0}^{p} \int dk'' \binom{p-1}{\mathcal{N}_\tau} \binom{p}{\mathcal{N}_\eta} P_\infty^p(k'', \tau_1\xi')$$

$$\times \Phi(\tau_1 + 2\mathcal{N}_\tau - p + 1, 2\mathcal{N}_\eta - p, m\xi'; k'', \hat{m}_0 + \hat{m}\tau_1\xi')$$

where $\mathcal{N}_\tau$ and $\mathcal{N}_\eta$ represent the number of neurons with states equal to +1 in the configurations of τ, η respectively.
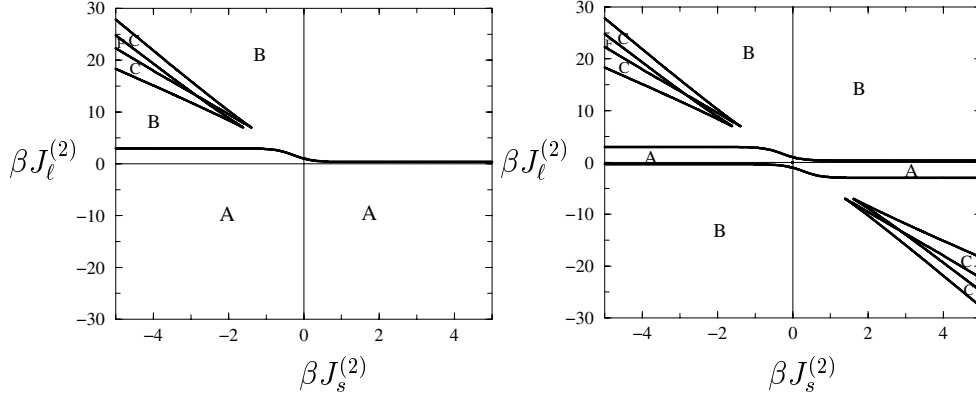
4.3. Phase diagrams

From this point onwards our discussion will cover both the sequential as well as the parallel case. In order to calculate phase transitions and draw phase diagrams we will first calculate the free-energy surfaces (16) and (30) which at this stage are still functions of the order parameters m and $\hat{m}$. For simplicity we will now set $\theta = 0$. The distributions $P_\infty^s(\cdots)$ and $P_\infty^p(\cdots)$ can be calculated numerically via iteration of (29) and (45), and bifurcations of the non-trivial values for the pure state overlap from the trivial solution (if they exist) will then be given as the solutions of the following fixed-point problems:

$$\begin{aligned} \text{sequential:} \quad & m = \partial_{i\hat{m}} F_{\text{seq}}(i\hat{m}) \qquad && \text{at} \quad i\hat{m} = -J_\ell^{(2)} m \\ \text{parallel:} \quad & m = \partial_{i\hat{m}} F_{\text{par}}(i\hat{m}, m) \qquad && \text{at} \quad i\hat{m} = \partial_m F_{\text{par}}(i\hat{m}, m) \end{aligned} \quad (46)$$

with

$$F_{\text{seq}}(i\hat{m}) = -\frac{1}{2\beta} \sum_{\lambda' \pm 1} \sum_{\mathcal{N}_\tau=0}^{p} \int dk' \binom{p}{\mathcal{N}_\tau} P_\infty^s(k', \lambda')$$

$$\times \log[e^{\beta[J_s^{(1)} + J_s^{(2)}(2\mathcal{N}_\tau - p)]} + e^{-\beta[J_s^{(1)} + J_s^{(2)}(2\mathcal{N}_\tau - p)]} k' e^{2\beta i\hat{m}\lambda'}] \quad (47)$$

Figure 4. Phase diagrams of model (4) for $p = 2$ and with $J_s^{(1)} = J_\ell^{(1)} = 0$, for sequential (left) and parallel dynamics (right). Lines separate regions with different numbers of locally stable solutions for the pure state overlap m, calculated from equations (47) and (48). In region A the only stable solution is the trivial one. The transition A $\to$ B is second order, whereas B $\to$ C and F $\to$ C are first order (see also figure 5). In regions B,C and F there are 1, 2 and 3 locally stable $m > 0$ states, respectively (see also free-energy graphs, figure 7).

$$F_{\mathrm{par}}(\mathrm{i}\hat{m}, m) = -\frac{1}{4\beta} \sum_{\tau_1 = \pm 1} \sum_{\xi' = \pm 1} \sum_{\mathcal{N}_\tau = 0}^{p-1} \sum_{\mathcal{N}_\eta = 0}^{p} \int \mathrm{d}k'' \binom{p-1}{\mathcal{N}_\tau} \binom{p}{\mathcal{N}_\eta} P_\infty^p(k'', \tau_1 \xi')$$
$$\times \log[2\cosh[\beta J_\ell^{(2)} m\xi' + 2\beta J_s^{(1)} + \beta J_s^{(2)}(\tau_1 - 2p + 2\mathcal{N}_\tau + 2\mathcal{N}_\eta + 1)]$$
$$+ 2\cosh[\beta J_\ell^{(2)} m\xi' + \beta J_s^{(2)}[2\mathcal{N}_\eta - 2\mathcal{N}_\tau + \tau_1 + 1]]k'' \mathrm{e}^{2\beta \mathrm{i}\hat{m}\tau_1 \xi'}]. \tag{48}$$

As in the solution of model (5) in section 3, the parallel dynamics fixed-point problem (46), (48) takes the form of a set of coupled equations, which makes the evaluation of bifurcation points essentially more laborious.

The solutions of the above equations, for $J_s^{(1)} = J_\ell^{(1)} = 0$ and for the simplest non-trivial case $p = 2$, are shown in the phase diagrams of figure 4. One distinguishes between four different regions, dependent on the number of locally stable 'pure state' solutions: region A with $m = 0$ only, region B with one locally stable $m > 0$ state (and one $m < 0$), regions C with two locally stable $m > 0$ states (and two $m < 0$ ones) and region F with three $m > 0$ states (and three $m < 0$ ones). Note that region F is created at the point where regions C start overlapping. The transition A $\to$ B is second order, whereas B $\to$ C and F $\to$ C are first order. The two qualitatively different types of bifurcations are also shown in figure 5 (left panel), where we draw the solution(s) of the overlap m as a function of βJ_ℓ along the line $\beta J_s = -1.8$ (a line crossing regions A, B and C). The zero noise region ($T = \beta^{-1} = 0$) for the phase diagram of figure 4 is shown in figure 5 (right panel) where we draw the transition lines separating recall regimes A, B, C and F in the $(J_\ell^{(2)}, T)$ plane for $J_s^{(2)} = -4$.

In equations (47) and (48) we observe that, due to the explicit appearance of the variable p in the solution of the overlap order parameter (which is due to short-range interactions, originating from expressions of the form $\exp[\beta(J_s^{(1)} + J_s^{(2)} \sum_{\mu=1}^p \xi_i^\mu \xi_{i+1}^\mu)]$, see e.g. (31)), it will no longer be true that the pure state ansatz leads to solutions which are independent of the number of stored patterns, as is the case for standard mean-field Hopfield networks. This is also shown in the phase diagrams of figure 6, which have been constructed from (47), (48) with $J_s^{(1)} = J_\ell^{(1)} = 0$ and for $p = 15$. We observe a significant increase in the number of transition
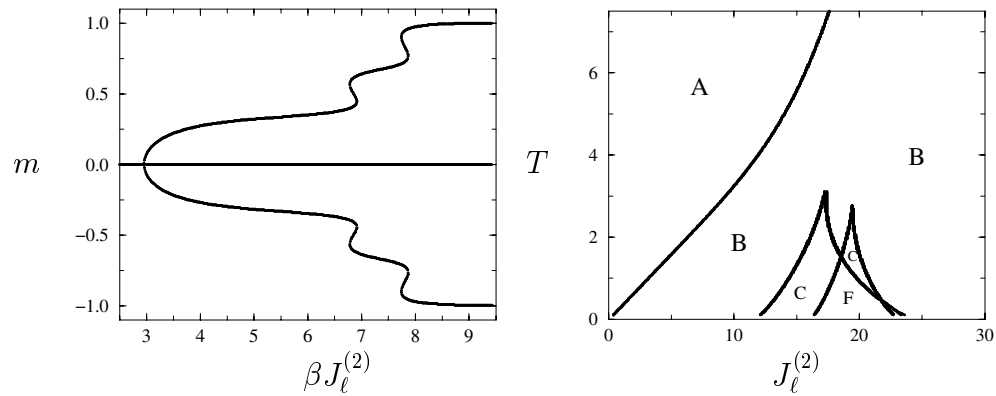
Figure 5. Left: sequential dynamics bifurcation diagram corresponding to the phase diagram of figure 4 along the line $\beta J_s^{(2)} = -1.8$. The transition A $\rightarrow$ B in figure 4 is shown here as a continuous bifurcation of the trivial solution whereas the two other bifurcations (at $\beta J_\ell^{(2)} \approx 6.76$ and $\beta J_\ell^{(2)} \approx 7.7$) correspond to the first-order transitions B $\rightarrow$ C. Right: alternative presentation of the phase diagram of figure 4 drawn in the $(J_\ell^{(2)}, T)$ plane (with $T = \beta^{-1}$) for $J_s^{(2)} = -4$.
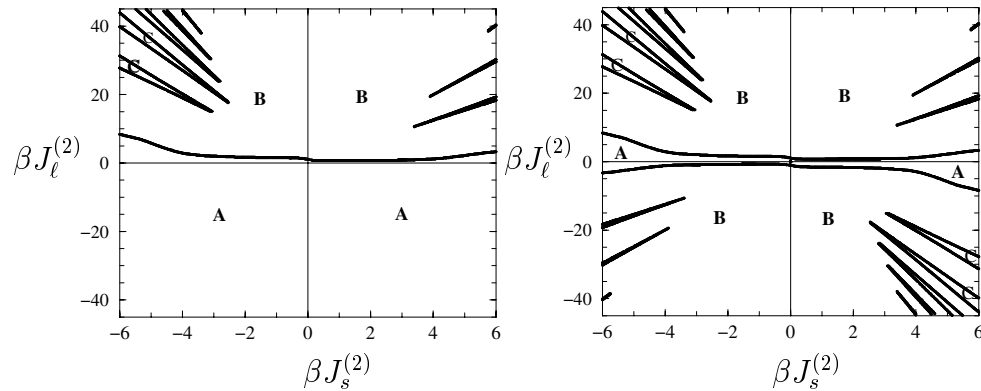
Figure 6. Phase diagrams of model (4) for $p = 15$ and with $J_\ell^{(1)} = J_s^{(1)} = 0$, for sequential dynamics (left) and parallel dynamics (right). Lines separate regions with different numbers of locally stable solutions of the pure state overlap m, calculated from equations (47) and (48). Compared with the cases $p = 1$ (figure 1) and $p = 2$ (figure 4), we observe a significant increase in the number of transition lines, caused by the explicit dependence of equations (47) and (48) on p. The diagrams involve three regions: region A where $m = 0$ only, region B with one $m > 0$ locally stable state and regions C (appearing inside each of the transition-line pairs) with two locally stable $m > 0$ states. The transition A $\rightarrow$ B is second order, whereas all transitions B $\rightarrow$ C are first order. Also note the appearance of further transition lines in the upper right quadrant, where $J_\ell^{(2)}, J_s^{(2)} > 0$ (and the lower left quadrant for the parallel dynamics case).

lines, as well as additional transition lines appearing in the quadrant $J_\ell^{(2)}, J_s^{(2)} > 0$ (and also in $J_\ell^{(2)}, J_s^{(2)} < 0$ for the parallel case). Such effects become more and more prominent as the number of patterns increases. It is also worth noting that figures 4 and 6 imply that all 'pairs' of first-order transition lines point to the origin of the $\{J_s^{(2)}, J_\ell^{(2)}\}$ plane.

Finally, due to the occurrence of imaginary saddle points in (46) and our strategy to eliminate the variable $\hat{m}$ by using the equation $\partial_m \phi(m, \hat{m}) = 0$, it need not be true that the saddle point with the lowest value of $\phi(m, \hat{m})$ is the minimum of ϕ (complex conjugation can

induce curvature sign changes, and in addition the minimum could occur at boundaries or as special limits). To remove this uncertainty we have evaluated the sequential dynamics free energy $\phi_{\text{seq}}(m, \hat{m})$ (16) after elimination of the conjugate variable $\hat{m}$ by using $\partial_m \phi(m, \hat{m}) = 0$ (middle row of figure 7) and $\partial_{\hat{m}} \phi(m, \hat{m}) = 0$ (lower row of figure 7) which shows that, although the convexity of the free-energy graphs is indeed affected, the location of the minima is not.

5. Benchmark tests

We now compare our results with simple benchmark cases. First, the solution of model (4) should reduce to the model of Amit *et al* [1], for regimes where $p \ll N$, upon removing short-range connectivity, i.e. for $J_s^{(1)} = J_s^{(2)} = 0$. Indeed we find that in this limit the probability distributions $P_\infty^{\text{seq}}(k)$ and $P_\infty^{\text{par}}(k)$ of the stochastic variables (22) and (39) both reduce to the delta peak: $\delta[k - 1]$. This simplifies the solution of our problem and allows us to write for the free energies

$$\phi_{\text{seq}}(m, \hat{m}) = -\mathrm{i}m_0\hat{m}_0 - \mathrm{i}m\hat{m} - m_0\theta$$
$$-\frac{1}{2}J_\ell^{(1)}m_0^2 - \frac{1}{2}J_\ell^{(2)}m^2 - \frac{1}{\beta}\langle\log 2\cosh[\beta\mathrm{i}(\hat{m}_0 + \hat{m}\xi)]\rangle_\xi$$

$$\phi_{\text{par}}(m, \hat{m}) = -\mathrm{i}m_0\hat{m}_0 - \mathrm{i}m\hat{m} - m_0\theta$$
$$-\frac{1}{\beta}\langle\log 2\cosh[\beta\mathrm{i}(\hat{m}_0 + \hat{m}\xi)]\rangle_\xi - \frac{1}{\beta}\langle\log 2\cosh[\beta(\theta + J_\ell^{(1)}m_0 + J_\ell^{(2)}m\xi)]\rangle_\xi.$$

Simple differentiation with respect to $\{m_0, \hat{m}_0, m, \hat{m}\}$ verifies that in the mean-field limit the pure order parameter solutions reduce to $m = \langle\xi\tanh[\beta(\theta + J_\ell^{(1)}m_0 + \xi J_\ell^{(2)}m)]\rangle_\xi$ and $m_0 = \langle\tanh[\beta(\theta + J_\ell^{(1)}m_0 + \xi J_\ell^{(2)}m)]\rangle_\xi$ as they should.

   Our second benchmark test is provided by the exact solution of model (5), section 3. We can immediately map model (4) to model (5) by setting $J_\ell^{(2)} = J_s^{(2)} = 0$. We then find that the key variables $\{k_j\}$ of equations (21) and (37) are given by a simple deterministic map. In fact, for both sequential and parallel dynamics we find that k_{seq} and k_{par} evolve towards the same fixed point

$$k = \mathrm{e}^{2\beta J_s}\mathrm{e}^{-\beta\mathrm{i}\hat{m}}\left[-\sinh[\beta\mathrm{i}\hat{m}] + \sqrt{\sinh^2[\beta\mathrm{i}\hat{m}] + \mathrm{e}^{-4\beta J_s}}\right]$$

which (at the relevant saddle points) can be verified to lead to the fixed-point equation (9) of model (5), namely

$$m = G(m; J_\ell, J_s) \qquad \text{with} \quad G(m; J_\ell, J_s) = \frac{\sinh[\beta J_\ell m]}{\sqrt{\sinh^2[\beta J_\ell m] + \mathrm{e}^{-4\beta J_s}}}.$$

   Thirdly, we have also compared the free energies of model (4), as given by our present solution, with that which one finds when using the alternative random-field technique of [15]. The latter relies on performing the spin summations in $R = \sum_\sigma \mathcal{F}(\sigma)$ (31) and deriving appropriate functions $A(\xi \cdot \xi')$ and $B(\xi \cdot \xi')$ such that the identity $\cosh[\beta(J_s(\xi \cdot \xi')\sigma' - \mathrm{i}\hat{m}\xi)] = \exp[\beta(A(\xi \cdot \xi')\sigma' + B(\xi \cdot \xi'))]$ is true for $\sigma' \in \{-1, 1\}$. For instance, for expression (31) of sequential dynamics this leads to

$$-\lim_{N\to\infty}\frac{1}{\beta N}\log R_{\text{seq}} = -\lim_{N\to\infty}\frac{1}{2\beta N}\sum_{i=1}^N\log[4\cosh[\beta(J_{i,i+1}^s + h_i)]\cosh[\beta(J_{i,i+1}^s - h_i)]]$$

where

$$h_{i+1} = \mathrm{i}\hat{m}\xi_{i+1} - \frac{1}{2}\log\left[\frac{\cosh[\beta(J_{i,i+1}^s - h_i)]}{\cosh[\beta(J_{i,i+1}^s + h_i)]}\right] \qquad J_{lk}^s = J_s^{(1)} + J_s^{(2)}\xi_l \cdot \xi_k$$

(with $h_1 = i\hat{m}\xi_1$) and is in complete agreement with the free energy as found from (16), (24), (27).

Finally, for the special case $J_s^{(1)} = J_\ell^{(1)} = J_\ell^{(2)} = 0$ and $p = 1$ (short-range bond disorder and absence of long-range interactions) our model reduces to the classical short-range random-bond Ising model [12], in which we expect the integrated density $\hat{P}_\infty(k)$ (29) to acquire, at least in certain parameter regions, the form of the highly non-analytic devil's staircase [13,14]. In this special case the density (29) reduces (at saddle points $\{i\hat{m}_0 = -\theta, i\hat{m} = 0\}$) to

$$\hat{P}_{i+1}(k, \lambda) = \frac{1}{2}\left\{\hat{P}_i\left(e^{2\beta\theta}\frac{ke^{\beta J_s\lambda} - e^{-\beta J_s\lambda}}{e^{\beta J_s\lambda} - ke^{-\beta J_s\lambda}}, 1\right) + \hat{P}_i\left(e^{2\beta\theta}\frac{ke^{-\beta J_s\lambda} - e^{\beta J_s\lambda}}{e^{-\beta J_s\lambda} - ke^{\beta J_s\lambda}}, -1\right)\right\}$$

where $\lambda = \pm 1$ represents bond-disorder. One can now prove by induction that if the identity $\hat{P}_i(k, 1) = \hat{P}_i(k, -1)$ is true then also $\hat{P}_{i+1}(k, 1) = \hat{P}_{i+1}(k, -1)$, so that (assuming ergodicity and uniqueness of the stationary density) the above expression reduces to a single recursive equation

$$\hat{P}_{i+1}(k) = \frac{1}{2}\left\{\hat{P}_i\left(e^{2\beta\theta}\frac{ke^{\beta J_s} - e^{-\beta J_s}}{e^{\beta J_s} - ke^{-\beta J_s}}\right) + \hat{P}_i\left(e^{2\beta\theta}\frac{ke^{-\beta J_s} - e^{\beta J_s}}{e^{-\beta J_s} - ke^{\beta J_s}}\right)\right\}$$

which is recognized as equation 10 of [12], upon a simple re-definition of our stochastic variables: $\{k_n = e^{-2\beta i\hat{m}_0}R_{n,\downarrow}/R_{n,\uparrow}\} \rightarrow \{e^{2\beta i\hat{m}_0}R_{n,\uparrow}/R_{n,\downarrow}\}$ in (21). In the present benchmark case we have also verified the identity found in [16] relating short-range random-field models between sequential and parallel dynamics, namely

$$\psi_{\text{seq}}(\psi_{\text{seq}}(k; \xi''\xi', \theta), \xi'\xi, \theta) = \psi_{\text{par}}(k; \xi''\xi', \xi'\xi, \theta)$$

(which is the key identity to prove that in the thermodynamic limit sequential and parallel random-field models lead to the same physical states). Here, $\psi_{\text{seq}}(\cdots)$ and $\psi_{\text{par}}(\cdots)$ correspond to the functions defined in (22) and (39). Indeed, functional iteration of (22) (with the saddle point requirements $i\hat{m}_0 = -\theta - J_\ell^{(1)}m_0$ and $i\hat{m} = -J_\ell^{(2)}m$) gives (39).

6. Theory versus simulations

In order to test our results further, we have performed extensive simulation experiments of the process (1), for model (4). In all cases the initial state is prepared randomly, with non-zero correlation only with pattern $\{\xi_i^1\}$. Our simulation results for the model which gives the phase diagram of figure 4 ($p = 2$ and $J_\ell^{(1)} = J_s^{(1)} = 0$) are shown in figure 7 (upper row) where we draw the equilibrium value of the recall overlap $m_1(t \rightarrow \infty)$ as a function of the initial state $m_1(t = 0)$. We have performed our experiments for three different regions of the phase diagram: region B (one $m > 0$ stable state), region C (two $m > 0$ stable states) and region F (three $m > 0$ stable states). In regions B and C the simulation experiments verify the appearance and location of multiple ergodic sectors; to compare with the theoretical results, see also the free-energy graphs in the middle and lower panels of figure 7. In region F the simulation experiments show that the system can enter only two possible domains of attraction (excluding thus the theoretically predicted state $m \approx 0.32$). This is due to (i) the system's finite size ($N = 1000$), in combination with (ii) the (relatively) small energy barrier separating the two physical states $m_a \approx 0.32$ and $m_b \approx 0.68$ (this allows the system to move from state m_a to m_b with a non-negligible probability). Our restriction to system size $N = 1000$ is prompted by the extremely long equilibration times (of the order of $\mathcal{O}(10^6)$ flips/spin). This, in turn, is due to domain formation: large clusters of neurons tend to freeze in specific configurations. As a consequence, in order for neurons to flip, the entire domain has to flip. In figure 8 (left graph) we show the value of the condensed overlap as a function of time in region F. We see that, starting

Region **C**   Region **F**   Region **B**
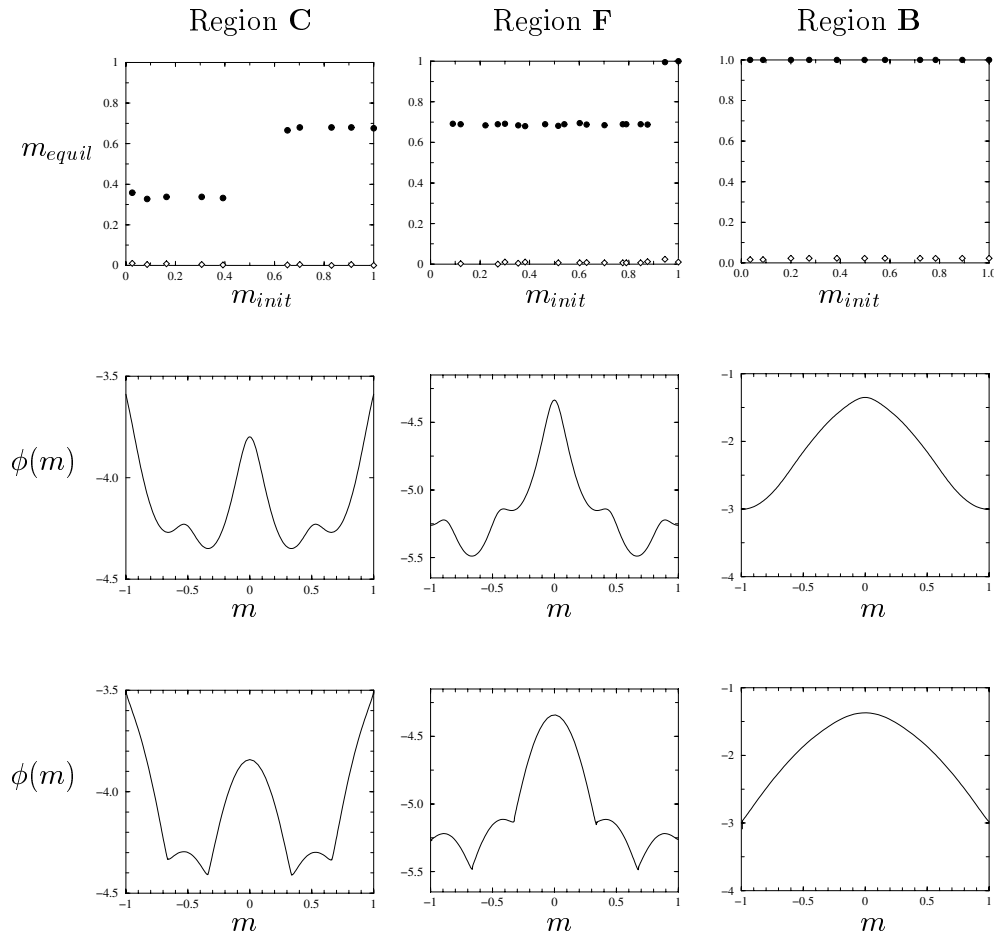
Figure 7. Upper row: sequential dynamics simulation results of the dynamical process (1), with model (4), for a system with $p = 2$ patterns. These were carried out in three different regions C, F and B of the phase diagram of figure 4. System size: $N = 1000$. Initial conditions are random, subject to prescribed correlations with pattern $\{\xi_i^1\}$. We show the equilibrium state $m(t \to \infty)$ of the 'pure state' overlap m_1 (full circles), as well as the overlap m_2 (open diamonds), as functions of the initial state $m(t = 0)$. Finite size effects are of the order $\mathcal{O}(N^{-1/2}) \approx 0.03$. Middle and lower rows: free energy per neuron $\phi_{\text{seq}}(m, i\hat{m})$, after elimination of the conjugate order parameter $\hat{m}$ via $\partial_m \phi_{\text{seq}}(m, i\hat{m}) = 0$ (middle row), and similarly after elimination of $\hat{m}$ via $\partial_{\hat{m}} \phi_{\text{seq}}(m, i\hat{m}) = 0$ (lower row). Left column: $\beta J_\ell^{(2)} = 14$ and $\beta J_s^{(2)} = -3.5$ (region C of the phase diagram of figure 4), middle column: $\beta J_\ell^{(2)} = 18.5$ and $\beta J_s^{(2)} = -4$ (region F), and right column: $\beta J_\ell^{(2)} = 8$ and $\beta J_s^{(2)} = -3.5$ (region B). For all graphs $J_\ell^{(1)} = J_s^{(1)} = 0$.

from an initial state $m_1(0) \approx 0.09$, the system gradually approaches the theoretically predicted locally stable state, where it indeed stays for a period of $\approx 4 \times 10^5$ flips/spin. Due to finite size effects, however, this state is thermodynamically unstable. A sudden transition to a new meta-stable state is then observed, generated by the flipping of entire domains. Equilibrium is reached in these simulations at about 2×10^6 flips/spin, where a second and final jump transition takes place. In the right graph of figure 8 we show a simulation experiment carried out in region C, starting from initial conditions $m_1(0) \approx 0.08$. Here equilibrium is reached after about 10^6 flips/spin, and due to a (relatively) high energy barrier separating the two $m > 0$
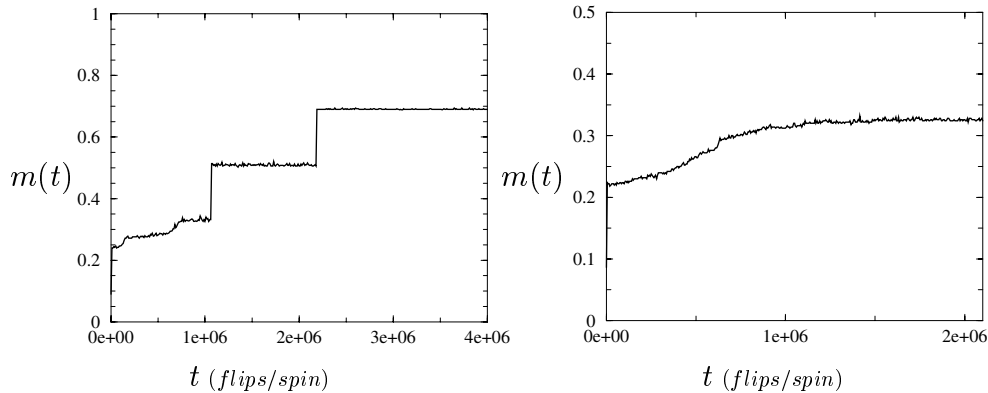
Figure 8. Simulation results for regions F (left) and C (right) of the phase diagram of figure 4. We show the evolution of the 'pure state' overlap order parameter as a function of time. In region F (left) the theory predicts a locally stable state at $m \approx 0.32$, which, due to finite size effects, appears here only as a meta-stable state. Two prominent jump transitions occur, until finally equilibrium is reached, at $m \approx 0.68$ (the jumps indicate domain-flipping). In region C (right) full equilibration still requires simulation times of the order of $\mathcal{O}(10^6)$ flips/spin, after which the result is in true agreement with the theory.

physical states (see energy graphs in regions C, left column of figure 7) there is no domain-related transition. In all our experiments the value of the non-selected pattern overlap $m_2(t)$ is found to remain zero (open diamond points), which justifies *a posteriori* our pure state ansatz.

7. Discussion

In this paper we have presented an exact equilibrium solution for a specific class of spatially structured Ising spin (attractor) neural network models, in which there is competition induced by the presence of two qualitatively different types of synaptic interactions: those operating only between nearest neighbours in a 1D chain (short range), and those operating between any pair of neurons (long range). The values taken by the interactions present are given by Hebbian-type rules, as in the more familiar mean-field attractor networks. We have solved these models by using a combination of mean- and random-field techniques for both sequential and parallel dynamics. As in the standard 1D RFIM-type models our expressions for the disorder-averaged free energy per neuron take the form of integrals over the distribution of a random variable, which represents the ratio of conditioned partition functions. This distribution can be evaluated numerically without much effort, and the key macroscopic observables then follow via simple differentiation.

 We found that there are regions in parameter space where information processing between the two types of synaptic interactions can induce phenomena which are quite novel in the arena of associative memory models, such as the appearance of multiple locally stable states, and of first-order transitions between them, even for finite p and upon making the 'pure state' ansatz. These peculiarities come to life particularly in regions where short- and long-range synapses compete most strongly, for instance, where one has Hebbian long-range interactions in combination with anti-Hebbian short-range ones, and they become more evident when increasing the number of stored patterns. Particularly in the upper left quadrant of parameter space $\{J_\ell > 0, J_s < 0\}$ one observes the appearance of an increasing number of dynamic transition lines (first- and second-order ones). This feature is in sharp contrast with the

conventional (infinite-range) Hopfield-like networks [1], where for finite p the 'pure state' ansatz automatically renders the remaining order parameter independent of the number of patterns stored. Phenomena such as simultaneous existence of multiple locally stable states (in which the quality of pattern recall depends crucially on initial conditions) can play a potentially useful role: poor cue signals can no longer evoke pattern recall. We also found that parallel dynamics transition lines in parameter space are exact reflection in the origin of those in sequential dynamics and that the relevant macroscopic observables can be obtained from those of sequential dynamics via simple transformations. One important analytical step here (parallel dynamics) has been the dimensionality reduction of the relevant stochastic process: we found that one can express the initially three stochastic components via a single one which allows for great analytical simplifications. Simulation experiments also show that the dynamics of the model are highly non-trivial, with plateaus and jump discontinuities, caused by complex domain formation and domain interaction, which would justify a study in itself.

In a similar fashion one could now also study more complicated systems, where (in addition to the long-range synapses) the short-range synapses reach beyond nearest neighbours. Such models can still be solved in one-dimension using the techniques employed here. A different type of generalization would be to allow for a type of competition between synapses which would correspond to having stored patterns with different (pattern dependent) embedding strengths, as in [20]. All these will be subjects of a future work.

Acknowledgment

References

[1]   Amit D J, Gutfreund H and Sompolinsky H 1985 *Phys. Rev.* A **32** 1007–18
[2]   Amit D J, Gutfreund H and Sompolinsky H 1985 *Phys. Rev. Lett.* **55** 1530–3
[3]   Domany E, van Hemmen J L and Schulten K (ed) 1991 *Models of Neural Networks I* (Berlin: Springer)
[4]   Coolen A C C, Laughton S N and Sherrington D 1996 *Phys. Rev.* B **53** 8184–7
[5]   Castellanos A, Coolen A C C and Viana L 1998 *J. Phys. A: Math. Gen.* **31** 6615–34
[6]   Domany E, van Hemmen J L and Schulten K (ed) 1994 *Models of Neural Networks II* (Berlin: Springer)
[7]   Canning A and Gardner E 1988 *J. Phys. A: Math. Gen.* **21** 3275–84
[8]   Noest A J 1988 *Europhys. Lett.* **6** 469–74
[9]   Domany E, Kinzel W and Meir R 1989 *J. Phys. A: Math. Gen.* **22** 2081–102
[10] Jonker H J J, Coolen A C C and Denier van der Gon J J 1993 *J. Phys. A: Math. Gen.* **26** 2549–71
[11] Coolen A C C and Viana L 1996 *J. Phys. A: Math. Gen.* **29** 7855–66
[12] Brandt U and Gross W 1978 *Z. Phys.* B **31** 237–45
[13] Bruinsma R and Aeppli G 1983 *Phys. Rev. Lett.* **50** 1494–7
[14] Aeppli G and Bruinsma R 1983 *Phys. Lett.* A **97** 117–20
[15] Rujan P 1978 *Physica* A **91** 549–62
[16] Skantzos N S and Coolen A C C 2000 *J. Phys. A: Math. Gen.* **33** 1841–55
[17] Peretto P 1984 *Biol. Cybern.* **50** 51–62
[18] Yeomans J M 1992 *Statistical Mechanics of Phase Transitions* (Oxford: Oxford University Press)
[19] Vieira A P and Goncalves L L 1999 *J. Magn. Magn. Mat.* **192** 177–90
[20] Viana L 1988 *J. Physique* **49** 167–74